A Theoretical Model for S_N1 Ionic Dissociations in Solution. 3. Analysis of *tert*-Butyl Halides

Jeffery R. Mathis, Hyung J. Kim,† and James T. Hynes*

Contribution from the Department of Chemistry and Biochemistry, University of Colorado, Boulder, Colorado 80309-0215

Received November 30, 1992

Abstract: The S_N1 activation free energies and transition-state structure for the series *tert*-butyl chloride, -bromide, and -iodide in several solvents over a wide polarity range are examined theoretically. The analysis is effected by using a two-state valence bond representation for the solute electronic structure, in combination with a two-dimensional free energy formalism in terms of the alkyl halide nuclear separation coordinate and a solvent coordinate. The calculated *tert*-butyl halide activation free energies are in good agreement with experiment. In a fixed solvent, a decreasing activation free energy trend is found (Cl > Br > I) as well as a decreasing transition-state ionic character. Both fixed solvent trends, and others, are shown to arise from a decreasing electronic coupling variation between the covalent and ionic solute valence bond states, in fundamental contrast with earlier interpretations. A Brønsted plot for the series in a fixed solvent shows a slope (greater than unity) which is consistent with the Hammond postulate. As solvent polarity increases, the calculated activation free energies decrease for the series, yet the trend of decreasing transition state solvent stabilization with increasing solvent polarity is exhibited by all three *tert*-butyl halides, confirming and extending earlier results [Kim, H. J.; Hynes, J. T. *J. Am. Chem. Soc.* **1992**, *114*, 10508, 10528]. This trend is at variance with the conventional Hughes–Ingold interpretation for increasing S_N1 reaction rates with increasing solvent polarity but is consistent with the Hammond postulate. An approximately linear correlation is established for the transition-state ionic character and a suitably defined measure of the *tert*-butyl halide bond extension at the transition state. In addition, it is also demonstrated how a Brønsted plot for each halide in solvents of different polarity, whose slope is shown analytically to be proportional to the square of the transition state ionic character, could be used as an experimental test of these unconventional predictions.

1. Introduction

There is a great deal of experimental[1-6] evidence supporting an initial unimolecular ionization as the rate determining step in solution phase S_N1 (and E1) reaction mechanisms of alkyl halides (RX):

$$RX \xrightarrow{k_1} R^+X^- \xrightarrow{k_s,k_e} \text{substitution and/or elimination products} \quad (1.1)$$

Here a theoretical investigation is conducted of the free energetics and solute electronic structure which influence the initial ionization step, using the *tert*-butyl (*t*-Bu) halides as model substrates:[7]

$$(CH_3)_3CX \rightarrow (CH_3)_3C^+X^- \qquad X = Cl, Br, I \quad (1.2)$$

This study of the *tert*-butyl halide series is motivated by the results of the first paper of this series,[8a] hereafter referred to as 1, where it was found that the transition state (TS) solvent stabilization for *t*-BuCl ionization actually decreased with increasing solvent polarity, and yet the activation free energy also decreased. This is in complete contrast to the conventional Hughes–Ingold[2-5] explanation for decreasing activation free energies with increasing solvent polarity, where an ionic TS is supposed to become more stabilized, which then is supposed to lower the activation barrier.

The formalism presented in 1 to describe the evolving solute electronic structure in solution is employed again here. It consists of a quantum two valence bond (VB) state Hamiltonian for the solute, together with a recently developed nonlinear Schrödinger equation approach[9] that properly accounts for the solvent polarizations *and* the coupling to the solute electronic structure and charge distribution. Discussion of the similarities and differences between this approach and the general VB perspective for reactions explored by Shaik and Pross,[10] and for related

† Present address: Department of Chemistry, Carnegie Mellon University, Pittsburgh, PA 15213-3890.

(1) Ogg, R. A., Jr.; Polanyi, M. *Trans. Faraday Soc.* **1935**, *31*, 604.

(2) (a) Abraham, M. H.; Abraham, R. J. *J. Chem. Soc., Perkin Trans. II* **1974**, 47. (b) Abraham, M. H. *J. Chem. Soc., Perkin Trans. II* **1992**, 1343. (c) Abraham, M. H. *J. Chem. Soc., Perkin Trans. II* **1973**, 1343. (d) Evans, A. G. *Trans. Faraday Soc.* **1946**, *42*, 719.

(3) (a) Dvorko, G. F.; Ponomareva, E. A.; Kulik, N. I. *Russ. Chem. Rev.* **1984**, *53*, 547. (b) Kulik, N. I.; Dvorko, G. F. *Org. React. (Tartu)* **1974**, *11*, 333. (c) Abraham, M. H.; Doherty, R. M.; Kamlet, M. J.; Harris, J. M.; Taft, R. W. *J. Chem. Soc., Perkin Trans. II* **1987**, 913. (d) Abraham, M. H.; Grellier, P. L.; Nasehzadeh, A.; Walker, R. A. C. *J. Chem. Soc., Perkin Trans. II* **1988**, 1717.

(4) (a) Gleave, J. L.; Hughes, E. D.; Ingold, C. K. *J. Chem. Soc.* **1935**, 236. (b) Hughes, E. D.; Ingold, C. K. *J. Chem. Soc.* **1935**, 244. (c) Hughes, E. D.; Ingold, C. K. *Trans. Faraday Soc.* **1941**, *37*, 657. (d) Dostrovski, I.; Hughes, E. D.; Ingold, C. K. *J. Chem. Soc. (London)* **1946**, 173. (e) Gelles, E.; Hughes, E. D.; Ingold, C. K. *J. Chem. Soc. (London)* **1954**, 2918. (f) Ingold, C. K. *Proc. Chem. Soc.* **1957**, 279. (g) Ingold, C. K. *J. Chem. Soc. (London)* **1963**, 265. (h) Ingold, C. K. *Structure and Mechanism in Organic Chemistry*, 2nd ed.; Cornell University: Ithaca, 1969.

(5) (a) Richard, J. P. *Adv. Carbocation Chem.* **1989**, *1*, 121. (b) Okamoto, K. *Adv. Carbocation Chem.* **1989**, *1*, 171. See also: Hoz, S. *Acta Chem. Scand.* **1992**, *46*, 503.

(6) In the absence of other reagents, an alkene is the major product in aprotic solvents. For some general reviews on the S_N1/E1 borderline, see: Winstein, S.; Cocivera, M. *J. Am. Chem. Soc.* **1963**, *85*, 1702. Goering, H.; Humski, K. *J. Org. Chem.* **1975**, *40*, 920. Nordlander, J. E.; Hamilton, J. B., Jr.; Wu, F. Y.-H.; Jindal, S. P. *J. Am. Chem. Soc.* **1976**, *98*, 6658. Seib, R. C.; Shiner, V. J.; Sendijarević, V.; Humski, K. *J. Am. Chem. Soc.* **1978**, *100*, 8133.

(7) Inclusion of *tert*-butyl fluoride (*t*-BuF) would complete the *tert*-butyl halide series. However, *t*-BuF does not readily undergo unimolecular ionization due to the stability of the C–F bond (~108 kcal/mol[28a]) and is difficult to work with.

(8) (a) Kim, H. J.; Hynes, J. T. *J. Am. Chem. Soc.* **1992**, *114*, 10508. (b) Kim, H. J.; Hynes, J. T. *J. Am. Chem. Soc.* **1992**, *114*, 10528.

(9) (a) Kim, H. J.; Hynes, J. T. *J. Chem. Phys.* **1992**, *96*, 5088. (b) In the context of the self-consistent field approximation, see: Kim, H. J.; Hynes, J. T. *J. Chem. Phys.* **1990**, *93*, 5194; **1990**, *93*, 5211; **1990**, *94*, 2736. (c) See, also: Hynes, J. T.; Kim, H. J.; Mathis, J. R.; Timoneda, J. J. i. *J. Mol. Liq.*, in press, for a brief review of the applications of the theory presented in (a).

0002-7863/93/1515-8248$04.00/0

approaches to S_N1 reactions,[1,11,12] as well as the extensive literature on electronic structure in solution can be found in 1. Implementation of the formalism generates a two-dimensional free energy surface, in terms of the reacting solute internuclear separation r and a collective solvent coordinate s,[8a,11c,12] upon which the ionizations eq 1.2 take place.

Solvent description is at the dielectric continuum level, which precludes[13,14] incorporating such molecular solvent features as, e.g., ordering around the reactant ("structure-making")[15] that increases the reactant state free energy via the accompanying decrease in entropy. This molecular solvent property is most pronounced in hydroxylic solvents[15]—water being the most notable, where hydrogen bonding is extensive. Our study is then confined to ionizations in aprotic solvents for which a continuum description is a reasonable approximation.[8] In fact, the calculated activation free energies presented here agree with the experimental values[3] to within ±1.5 kcal/mol for all three *tert*-butyl halides in all solvents studied.

As was emphasized in 1, it is only the initial ionization step in eq 1.1 for which our formalism is intended to apply. The subsequent fate of the ion-pair intermediate, either substitution (S_N1) or elimination (E1),[6] is beyond our focus. (However, even in polar and nonpolar aprotic solvents, the S_N1 mechanism proper is followed if a suitable reagent is present in sufficient concentration[6]). In this sense, eq 1.2 can be regarded as a sort of limiting S_N1 behavior, and it is in this sense that we will refer to eq 1.2 as an S_N1 ionization.[8a]

The outline of this paper is as follows. Section 2 introduces the formulation used to describe the *tert*-butyl halide ionization process. Only enough detail to make the present paper self-contained is presented; refs 8 and 9 should be consulted for a full exposition. In section 3 the various vacuum potentials are given and discussed. Ionization transition-state structure and location trends for both fixed and varying solvent polarity are given in section 4 and analyzed in section 5. Concluding remarks are offered in section 6.

2. Theoretical Formulation

As in 1, a diabatic two VB state basis set, which depends parametrically on the internuclear separation r between the central carbon of the *tert*-butyl group and the departing halogen, is used to describe the solute electronic structure. Its members represent the reactant and product: a pure covalent VB state $\phi_C(r)[RX]$ and a pure ionic VB state $\phi_I(r)[R^+X^-]$. In the covalent state ϕ_C, the transferring electron occupies an orbital associated with the central carbon of the *tert*-butyl group, and for the higher energy ionic state ϕ_I, an orbital associated with the halogen. In general, ϕ_C and ϕ_I are not orthogonal, and the overlap integral

$$S(r) = \langle \phi_C(r) | \phi_I(r) \rangle \tag{2.1}$$

changes with r. It is thus convenient to use an orthonormal basis set

$$\psi_C(r) = \phi_C(r); \psi_I(r) = [1 - S^2(r)]^{-1/2}[\phi_I(r) - S(r)\phi_C(r)] \tag{2.2}$$

where $\psi_C(r)$ is the pure covalent state and $\psi_I(r)$ will be associated with the ionic state. As displayed above, $\psi_I(r)$ is actually a mixed state; however its partial covalent character is approximately assessed[8a] as $\approx S^2(r)$, which is negligible except at $r \approx r_g$, the vacuum equilibrium R–X bond length.[8a] Thus $\psi_I(r)$ will be referred to as the ionic state.

In this orthonormal basis, the r-dependent vacuum Hamiltonian becomes

$$\mathcal{H}^0(r) = \begin{bmatrix} V_C^0(r) & -\beta(r) \\ -\beta(r) & V_I^0(r) \end{bmatrix} \tag{2.3}$$

where $V_C^0(r)$ and $V_I^0(r)$ are the covalent and ionic potential energy curves in vacuum, and $\beta(r)$ is the vacuum electronic coupling in the orthonormal basis. The matrix elements in the orthonormal and diabatic bases are related by

$$V_C^0(r) = \mathcal{H}_{11}^0(r)$$

$$V_I^0(r) = [1 - S^2(r)]^{-1}\,[\mathcal{H}_{22}^0(r) - 2S(r)\mathcal{H}_{12}^0(r) + S^2(r)\mathcal{H}_{11}^0(r)] \tag{2.4}$$

$$-\beta(r) = [1 - S^2(r)]^{-1/2}\,[\mathcal{H}_{12}^0(r) - S(r)\mathcal{H}_{11}^0(r)]$$

with $\mathcal{H}_{ij}^0$ the vacuum matrix elements in the diabatic basis. The $r \to \infty$ energy difference between V_I^0 and V_C^0 is the *tert*-butyl radical ionization potential minus the (positive) halogen electron affinity. The electronically adiabatic ground and excited states in this representation are given by the eigenstates of the matrix eq 2.3.

When a *tert*-butyl halide is immersed in a polar solvent, the ionic state ψ_I will become stabilized relative to the covalent state ψ_C, due to electrostatic interactions between the solute ionic charge distribution and the solvent polarizations. The stabilization magnitude depends not only on the solvent polarity but also on the extent to which the solvent polarizations have adjusted to the existing solute charge distribution. Ogg and Polanyi,[1] in their initial description of ionization processes, also couched their analysis in terms of covalent and ionic valence bond states. But they assumed that all the solvent polarizations were in equilibrium with the ionic state charge distribution, i.e., equilibrium solvation of the ionic state at all separations r. These two states were then imagined to be subsequently diagonalized, and the resulting lower electronically adiabatic, one-dimensional free energy surface was to be viewed as the surface upon which the ionization took place. One fundamental problem with this approach—among others[8]—is that the solvent polarizations are always equilibrated to the ionic valence bond state, even in the presence of electronic coupling. This diagonalization procedure fails to allow the solvent polarizations to adjust to the solute's evolving charge distribution,[8,9] and an alternative and more general approach is necessary.

In the formalism of Kim and Hynes,[9] the solvent interacts with the solute charge distribution via two types of polarizations: the electronic polarization $\vec{P}_{el}$ associated with the solvent electrons' motion, and the orientational polarization $\vec{P}_{or}$ associated with rotations (and translations) of the individual solvent molecules. $\vec{P}_{el}$ always maintains an equilibrium with the solute,[9] but $\vec{P}_{or}$ is in general out of equilibrium: the solute electronic motion time scale is in general much faster[9a] than that for $\vec{P}_{or}$. The solvation free energies associated with both $\vec{P}_{el}$ and $\vec{P}_{or}$ depend on the solute charge distribution and thus will be r-dependent.

The $\vec{P}_{or}$-dependent ionic stabilization can be characterized by an effective solvent coordinate s

$$\vec{P}_{or} = \frac{1}{4\pi}\left(\frac{1}{\epsilon_\infty} - \frac{1}{\epsilon_0}\right)\epsilon_\infty[s\vec{\mathcal{E}}_I + (1-s)\vec{\mathcal{E}}_C] \tag{2.5}$$

where ϵ_∞ and ϵ_0 are the solvent optical and static dielectric

(10) Pross, A.; Shaik, S. S. *Acc. Chem. Res.* **1983**, *16*, 363. Pross, A.; Shaik, S. S. *Tetrahedron Lett.* **1982**, *23*, 5467; Shaik, S. S. *Prog. Phys. Org. Chem.* **1985**, *15*, 191. Shaik, S. S. *J. Org. Chem.* **1987**, *52*, 1563. Pross, A. *Acc. Chem. Res.* **1985**, *18*, 212.

(11) (a) For an empirical valence bond (EVB) approach in connection with S_N1 reactions, see, e.g.: Warshel, A.; Weiss, R. M. *J. Am. Chem. Soc.* **1980**, *102*, 6218. Warshel, A. *Acc. Chem. Res.* **1981**, *14*, 284; Warshel, A. *J. Phys. Chem.* **1982**, *86*, 2218. Figure 2.3 in Warshel, A. *Computer Modeling of Chemical Reactions in Enzymes and Solutions*; Wiley and Sons, Inc.: New York, 1991. (b) Zichi, D. A.; Hynes, J. T. *J. Chem. Phys.* **1988**, *88*, 2513. (c) Timoneda, J. J. i.; Hynes, J. T. *J. Phys. Chem.* **1991**, *95*, 10431.

(12) Lee, S.; Hynes, J. T. *J. Chem. Phys.* **1988**, *88*, 6853.

(13) Keirstead, W.; Wilson, K. R.; Hynes, J. T. *J. Chem. Phys.* **1991**, *95*, 5256. Carter, E. A.; Hynes, J. T. *J. Phys. Chem.* **1989**, *93*, 2184.

(14) Morita, T.; Ladanyi, B. M.; Hynes, J. T. *J. Phys.* 4Chem. **1989**, *93*, 1386.

(15) See, e.g.: Arnett, E. M. In *Physico-Chemical Processes in Mixed Aqueous Solvents*; Franks, F., Ed.; American Elsevier: New York, 1967. Franks, F.; Reid, D. S. In *Water: A Comprehensive Treatise*; Franks, F. Ed.; Plenum: New York, 1973; Vol. 2.

constants, and $\mathcal{E}_I$ and $\mathcal{E}_C$ are the vacuum electric fields arising from the solute ionic and covalent states, ψ_I and ψ_C, respectively.[8a,11c,12] $\vec{P}_{or}$ is completely equilibrated when $s = 0$ to the covalent state charge distribution, and when $s = 1$, to the ionic state charge distribution. The problem is simplified[8a] by assuming that the ionic state permanent dipole moment is much larger than its (negligible) counterpart for the pure covalent state.[16]

The fully quantum mechanical treatment of the solvent electronic polarization $\vec{P}_{el}$ has been extensively discussed elsewhere,[8,9] and only the required main results will be given here. For the present two VB state basis set, one makes the ansatz for the *t*-BuX reaction system wave function

$$\Psi(r, s) = c_C(r, s)\psi_C(r) + c_I(r, s)\psi_I(r) \tag{2.6}$$

By invoking the variational principle[9a] that the actual solute wave function is the one which minimizes the free energy, a Schrödinger equation for Ψ is obtained, the exact form of which is not needed here, and is given in ref 9a. The Schrödinger equation is, in general, nonlinear in Ψ due to the electrostatic interaction between the *t*-BuX solute and the equilibrated $\vec{P}_{el}$, which itself depends on Ψ. Using Ψ obtained from the Schrödinger equation in ref 9a, the general free energy function is then given by[8,9a]

$$G(r, s) = \bar{V}(r, s) - \frac{1}{2}\Delta V(r, s)x - \beta(r)y + \frac{1}{4}\Delta G_r^{el}(r)y^2 f + \Delta G_r(r)s^2 - k_B T \ln [r/r_0]^2$$

$$f \equiv \frac{\rho}{y + \rho} \tag{2.7}$$

where

$$\bar{V}(r, s) = \frac{1}{2}(V_C^0(r) + V_I^0(r) - \Delta G_r^{el}(r) - 2\Delta G_r(r)s) \tag{2.8}$$

$$\Delta V(r, s) = V_I^0(r) - \Delta G_r^{el}(r) - 2\Delta G_r(r)s - V_C^0(r)$$

Here $\Delta G_r(r)$ is the solvent reorganization free energy measuring the ultimate free energy change subsequent to a Franck–Condon transition $\psi_C \rightarrow \psi_I$ at a given r and is also the negative of the free energy of solvation associated with $\vec{P}_{or}$. Similarly, $\Delta G_r^{el}(r)$ is the negative of the solvation free energy associated with $\vec{P}_{el}$ and could also be regarded as an electronic polarization reorganization free energy in a purely hypothetical situation where $\vec{P}_{el}$ motion was slow. As in 1, we write

$$\Delta G_r(r) = \left(\frac{1}{\epsilon_\infty} - \frac{1}{\epsilon_0}\right)M_s(r) \qquad \Delta G_r^{el}(r) = \left(1 - \frac{1}{\epsilon_\infty}\right)M_s(r) \tag{2.9}$$

$$M_s(r) \equiv \frac{1}{8\pi}\int_V d\tilde{x}\,\mathcal{E}_I(\tilde{x};r)\cdot\mathcal{E}_I(\tilde{x};r)$$

where $M_s(r)$ is the electrostatic energy associated with the ionic electric field $\mathcal{E}_I$ in the orthonormal basis.[8,11c] At large separations, $M_s(r)$ resembles the $1/r$-dependent Marcus[17,18] expression and is smoothly extrapolated to zero according to the prescription of Zichi and Hynes[11b] in the limit of zero separation. The evaluation of $M_s(r)$ is a technical point, and the reader is referred to ref 11b for the details. The last term in eq 2.7 is a temperature-dependent centrifugal term associated with the *tert*-butyl halide rotation referenced to the covalent state equilibrium bond length r_0.[8a,19]

The dimensionless parameter

$$\rho(r) = \frac{2\beta(r)}{\hbar\omega_{el}} \tag{2.10}$$

is a measure of the time scales associated with the solute electronic motion—as gauged by the solute electronic coupling $\beta(r)$, and with the solvent electronic polarization $\vec{P}_{el}$—as gauged by the electronic polarization response frequency ω_{el}. The factor f in eq 2.7 represents these time scales and is given by $f = (\tau_{el} + \tau_{tr})^{-1}\tau_{el}$, where τ_{el} is the time scale for $\vec{P}_{el}$ motion and τ_{tr} is the time scale for the transferring solute electron.[8a,9a] When $\rho \rightarrow 0, f \rightarrow 0$, $\vec{P}_{el}$ adjusts instantaneously to a pointlike and hence much slower solute electron, while when $\rho \rightarrow \infty, f \rightarrow 1$, the solute electronic motion is much faster than the $\vec{P}_{el}$ response, so $\vec{P}_{el}$ adjusts to a quantum averaged solute charge distribution. x and y in eq 2.7 are convenient variables that represent the two state coefficients (c_C, c_I) via

$$x \equiv c_C^2 - c_I^2 \qquad y \equiv 2c_C c_I \tag{2.11}$$

$$x^2 + y^2 = 1$$

where the (r, s) notation in eq 2.6 has been suppressed. Both x and y have values ranging from -1 to 1. The case $x = 1$ and $y = 0$ corresponds to the completely covalent *t*-BuX reactant state, while $x = -1, y = 0$ is the completely ionic *t*-Bu$^+$X$^-$ product state. The case $x = 0, y = 1$ corresponds to a completely delocalized intermediate state between the two reactant and product extremes ($y < 0$ describes the higher energy antisymmetric state not relevant here[9a,b]). x and y are found by solving

$$2\beta(r)x - \Delta V(r, s)y = \Delta G_r^{el}(r)xy\frac{f(1 + f)}{2} \tag{2.12}$$

obtained from the nonlinear Schrödinger equation in ref 9a.

The solution of eq 2.12 gives the solute charge distribution, i.e., the solute electronic structure, for any point (r, s) and thus the charge distribution and free energy $G(r, s)$ (eq 2.7) for nonequilibrium solvation states.[8a,9] For the special case of equilibrium solvation

$$\frac{\partial G(r, s)}{\partial s} = 0 \tag{2.13}$$

it follows directly from eq 2.7 that

$$s_{eq} = \left(\frac{1 - x_{eq}}{2}\right) = c_I^2 \tag{2.14}$$

Thus, when the solvent is in equilibrium with the solute at a given r, the value of the solvent coordinate is exactly the solute ionic character. Insertion of eq 2.14 into eq 2.12 results in a polynomial equation whose solutions $(x_{eq}(r), y_{eq}(r))$ describe the solute electronic structure and the solvent polarizations of the equilibrium solvation states.[20] The r-dependent equilibrium free energy $G_{eq}(r) = G(r, s_{eq}(r))$ is obtained by substituting eq 2.14 into eq 2.12 and combining with eq 2.7. Equations 2.7, 2.12, and 2.14 are then the fundamental equations used to calculate the free energy surfaces in section 4.

3. Model Specifics for the *tert*-Butyl Halides

In this section we describe the machinery necessary for the specific implementation of the theory in section 2. This entails

(16) There is, in general, a covalent state dipole moment.[24,39-41] However, its magnitude (~1–2 Debye) is much smaller than the pure ionic state dipole (~9–10 Debye) in the vicinity of the vacuum equilibrium bond length r_g.

(17) Marcus, R. A. *J. Chem. Phys.* **1956**, *24*, 966; **1956**, *24*, 979; *Faraday Disc. Chem. Soc.* **1960**, *29*, 21; **1960**, *29*, 29; *J. Chem. Phys.* **1963**, *3*, 1858; *Ann. Rev. Phys. Chem.* **1964**, *15*, 155.

(18) Marcus, R. A.; Sutin, N. *Biochim. Biophys. Acta* **1985**, *811*, 265.

(19) Sceats, M. *Adv. Chem. Phys.* **1988**, 70, 357. As in ref 8a, the time-dependent dielectric friction effect on the solute rotational motion is neglected.

(20) The algebraic equation obtained from the Born–Oppenheimer (BO) Schrödinger equation in ref 9a that determines the state coefficients is given by the $\rho = 0$, f = 0 version of eq 2.12: $2\beta(r)x - \Delta V(r,s)y = 0$. The self-consistent[9] (SC) version is obtained from eq 2.12 by letting $\rho \rightarrow \infty$, f $\rightarrow$ 1: $2\beta(r)x - \Delta V(r,s)y = \Delta G_r^{el}(r)xy$. The equilibrium versions of each of these are readily obtainable using eq 2.14. For the BO case, $x_{eq}(y_{eq} - 2\beta(r)/\Delta G_r(r)) = -(\Delta G^{eq}(r)/\Delta G_r(r))y_{eq}$ and in the SC case

$$x_{eq}\left(y_{eq} - \frac{2\beta(r)}{(\Delta g_r(r) + \Delta G_r^{el}(r))}\right) = -\left(\frac{\Delta G^e{}_q(r)}{(\Delta G_r(r) + \Delta G_r^{el}(r))}\right)y_{eq}$$

Here $\Delta G^{eq}(r)$ is the difference in the completely equilibrated ionic potential, $\Delta G^{eq}(r) = V_I^0(r) - \Delta G_r(r) - \Delta G_r^{el}(r) - V_C^0(r)$. See ref 9 for explicit details of these Schrödinger equations.

Table I. Vacuum Ionic State Parameters[a-c]

	t-BuCl	*t*-BuBr	*t*-BuI
a_1 (kcal/mol)	0.331	0.369	0.429
a_2 (kcal/mol)	0.468	0.522	0.607
b_1 (Å)	3.034	3.118	3.235
b_2 (Å)	3.503	3.600	3.735
EA (kcal/mol)	83.37	77.58	70.58

[a] LJ parameters a_i and b_i taken from refs 21 and 23a. [b] *EA*'s taken from ref 23b. [c] *tert*-Butyl radical ionization potential used is 165.0 kcal/mol.[22]

the introduction of (a) the vacuum ionic, covalent, and adiabatic ground-state potential energy functions and (b) the form of the wave functions used to represent the VB covalent and ionic states, and the method used to calculate the electronic coupling between them. For completeness and clarity of comparison between the three halide systems, the *t*-BuCl calculation[8] has been repeated with the new parameter set to be described presently.

A. Vacuum Potential Energy Functions. This work employs the same vacuum potential energy functional forms used in 1 but with different parameters. The ionic potential energy, $\mathcal{H}^0_{22}(r)$, for all three halides is based on a model by Jorgensen et al. for a *tert*-butyl cation and a chloride anion,[21] consisting of short range Lennard–Jones (LJ) repulsions and long range Coulombic attractions. The *tert*-butyl cation is assumed to be a planar complex with C_3 symmetry and a carbon–methyl bond length l of 1.475 Å. Each of the three methyl groups is positively charged with $+0.2e$ and the central carbon with $+0.4e$. The halide anion is restricted to move along the C_3 symmetry axis. Furthermore, the planar geometry of the *tert*-butyl cation is assumed to be maintained during the entire ionization process; thus the change in the hybridization of the central carbon is not explicitly accounted for. This important point will be addressed in section 3B. $\mathcal{H}^0_{22}(r)$ is

$$\mathcal{H}^0_{22}(r) = a_1\left[\left(\frac{b_1}{r}\right)^{12} - \left(\frac{b_1}{r}\right)^{6}\right] - \frac{0.4e^2}{r} + 3a_2\left[\left(\frac{b_2^2}{r^2+l^2}\right)^{6} - \left(\frac{b_2^2}{r^2+l^2}\right)^{3}\right] - \frac{0.6e^2}{\sqrt{r^2+l^2}} + \Delta \quad (3.1)$$

Here Δ is the difference in the *tert*-butyl radical ionization potential (165.0 kcal/mol[22]) and the (positively defined) halogen electron affinity. The geometric mean combination method[23a] is used to generate the LJ parameters (a_1, a_2, b_1, b_2) from the halogen–halogen and *tert*-butyl–*tert*-butyl LJ parameters. The values for all parameters employed in the ionic potentials were taken from refs 21 and 23 and are compiled in Table I.

For the pure covalent curve $\mathcal{H}^0_{11}(r)$, a simple Morse potential is used

$$\mathcal{H}^0_{11}(r) = D_0\{\exp[-2a_0(r-r_0)] - 2\exp[-a_0(r-r_0)]\} \quad (3.2)$$

where r_0 is the covalent equilibrium bond length, D_0 is the covalent well depth at r_0 (the covalent bond dissociation energy (BDE)),

Table II. Covalent and Ground-State Parameters

	t-BuCl	*t*-BuBr	*t*-BuI
D_0 (kcal/mol)	65.5	57.9	51.2
D (kcal/mol)[a]	81.8	67.7	52.1
ICRE (kcal/mol)	16.3	9.8	0.9
$\gamma(r_g)$	0.19	0.17	0.06
$V^0_I(r_g) - V^0_C(r_g)$ (kcal/mol)[b]	487.4	335.0	219.8
BDE_{X-X} (kcal/mol)[c]	59.0	46.1	36.1
$k_0 = k$ (mdyne/Å)[d]	2.8	2.4	2.0
$r_0 = r_g$ (Å)[d]	1.80	1.96	2.16
a_0 (Å^{-1})	1.75	1.73	1.68
a (Å^{-1})	1.57	1.60	1.66

[a] Reference 28a. [b] The rather large diabatic gap near the reactant separation r_g is due to the steep repulsive behavior of the R^+–X^- interaction in this region. [c] Reference 28b. [d] Reference 29.

and a_0 is a measure of the curvature; near the minimum of $\mathcal{H}^0_{11}(r)$, the covalent stretching force constant, k_0, is related to a_0 by $a_0 = \sqrt{k_0/2D_0}$. These parameters must be determined by some independent means, as no experimental information is available. The procedure commonly employed[24] for pure covalent potential curves is to use (a) Pauling's geometric mean[24,25a] for D_0, (b) the sum of the covalent radii of each of the participating atoms in the bond for r_0, and (c) Badger's[26] empirical combination rule for k_0. Instead, here r_0 and k_0 are assumed to be the same as the experimentally determined values for the adiabatic ground state,[8a,27] k and r_g. D_0 turns out to be the most important quantity in the covalent potential, since its value directly affects the electronic coupling $\mathcal{H}^0_{12}$. The *tert*-butyl–*tert*-butyl BDE used in calculating D_0 is 72.7 kcal/mol,[28a] and the halogen–halogen BDEs were taken from ref 28b. The covalent-state parameters for the three halides are compiled in Table II.

Finally, the vacuum electronically adiabatic ground state of the halide systems can be well approximated by a Morse potential

$$E_g(r) = D\{\exp[-2a(r-r_g)] - 2\exp[-a(r-r_g)]\} \quad (3.3)$$

where r_g is the vacuum equilibrium bond length, D is the carbon–halogen BDE, and a is related to the carbon–halogen ground vibrational state stretching force constant k via $a = \sqrt{k/2D}$. These Morse potential parameters can be determined from experimental data and are taken from refs 28 and 29 (cf. Table II).

B. Wave Functions and Electronic Coupling. The electronic coupling $\mathcal{H}^0_{12}(r)$ is related to the pure covalent curve $\mathcal{H}^0_{11}(r)$ the pure ionic curve $\mathcal{H}^0_{22}(r)$, and the electronically adiabatic ground-state potential energy $E_g(r)$ by

$$-\mathcal{H}^0_{12}(r) = [(\mathcal{H}^0_{11}(r) - E_g(r))\,(\mathcal{H}^0_{22}(r) - E_g(r))]^{1/2} - E_g(r)S(r) \quad (3.4)$$

the secular equation for the gas-phase Schrödinger equation in the nonorthogonal diabatic basis $\{\phi_C, \phi_I\}$. The diagonal elements $V^0_C(r)$, $V^0_I(r)$ and the electronic coupling $\beta(r)$ for the vacuum

(21) Jorgenson, W. L.; Buckner, J. K.; Huston, S. E.; Rossky, P. J. *J. Am. Chem. Soc.* **1987**, *109*, 1891.

(22) If literature values of (a) 154.5 kcal/mol [Luo, Y.-R.; Pacey, P. D. *J. Phys. Chem.* **1991**, *95*, 9470] or (b) 159.74 kcal/mol [Screttas, C. G. *J. Org. Chem.* **1980**, *45*, 333] are used, H^0_{22}'s for *t*-BuCl and *t*-BuBr are actually lower than their respective adiabatic ground-state energies near $r \approx 3$–3.5 Å (therefore beyond the TS), which should never be the case. The *tert*-butyl radical ionization potential must then be increased. This results in a "dip" in the coupling curve for *t*-BuCl in Figure 2a, since the difference in the adiabatic ground state E_g and the ionic potential H^0_{22} for it is close to zero for $r \approx 2.7$–3 Å. However, the TS is located well before this region (cf. section 4). For *t*-BuBr, the ionization potential increase is large enough so that H^0_{22} is relatively far from E_g, and no dip is observed (H^0_{22} for *t*-BuI is not lower than its E_g). 165.0 kcal/mol is adopted for all *tert*-butyl halides to maintain consistency.

(23) (a) Wiese, H.; Brickmann, J. *Ber. Buns. Phys. Chem.* **1989**, *93*, 1464. (b) Hotop, H.; Lineberger, W. C. *J. Phys. Chem. Ref. Data* **1975**, *4*, 539.

(24) (a) Pauling, L. *The Nature of the Chemical Bond*, 2nd ed.; Cornell University: Ithaca, 1942. (b) Coulson, C. A. *Valence*, 2nd ed.; Oxford University Press: London, 1961.

(25) (a) Pauling, L.; Sherman, J. *J. Am. Chem. Soc.* **1937**, *59*, 1450. (b) Pauling, L.; Youst, D. M. *Proc. Natl. Acad. Sci. U.S.A.* **1932**, *18*, 414. (c) Pauling, L. *J. Am. Chem. Soc.* **1932**, *54*, 3570.

(26) Badger, R. M. *J. Chem. Phys.* **1934**, *2*, 128; **1935**, *3*, 710.

(27) (a) This is a common approximation. See, e.g., Warshell and Weiss in ref 11a. Coulson, C. A.; Danielson, U. *Arkiv Fysik* **1954**, *8*, 245. (b) If one used the respective covalent radii, one obtains $r^{Cl}_0 = 1.76$, $r^{Br}_0 = 1.91$, $r^{I}_0 = 2.10$ Å, which is not significantly different from the actual values. Covalent radii obtained from Huheey, J. *Inorganic Chemistry*, 3rd ed.; Harper and Row: New York, 1983.

(28) (a) Griller, D.; Kanabus-Kaminska, J. M.; Maccoll, A. *J. Mol. Struct.* **1988**, *163*, 125. (b) Hubert, K. P.; Herzberg, G. *Molecular Spectra and Molecular Structure Constants of Diatomic Molecules*; Van Nostrand: New York, 1979.

Hamiltonian in the orthonormal basis $\{\psi_C, \psi_I\}$ can then be evaluated using eq 2.4, once the overlap $S(r)$ is known.[30]

As mentioned above, the planar geometry of the *tert*-butyl cation is assumed to be maintained during the entire ionization process. The central carbon is thus constrained to sp^2 hybridization, and the diabatic wave functions $\{\phi_C, \phi_I\}$ can be approximated as two-electron spin singlet states composed only of p orbitals:

$$\phi_C \approx 2^{-1/2}[1 + \langle 2p_c\sigma|Np_x\sigma\rangle^2]^{-1/2}[2p_c\sigma(1)Np_x\sigma(2) + 2p_c\sigma(2)Np_x\sigma(1)] \quad (3.5)$$

$$\phi_I \approx Np_x\sigma(1)Np_x\sigma(2)$$

Here $2p_c\sigma$ and $Np_x\sigma$ are, respectively, the 2p carbon and Np ($N = 3, 4, 5$; X = Cl, Br, I) halogen atomic orbitals with σ symmetry. The overlap integrals $S(r)$ (cf. eq 2.1) for the three halides are evaluated with the approximations of Mulliken et al.[31]

This completes the prescription for the calculation of the vacuum Hamiltonian matrix elements. The numerical results are displayed in Figures 1 and 2. Notice the coupling trend in Figure 2a for $r \lesssim 3$ Å: $\beta_{Cl}(r) > \beta_{Br}(r) > \beta_I(r)$.[22] As will be demonstrated and explained, this coupling trend is ultimately responsible for all of the fixed solvent TS energetic and location trends for the *tert*-butyl halide series.

Before beginning an examination of the coupling trends, a comment is in order concerning the approximation of nonchanging central carbon hybridization. At the reactant geometry, the central carbon is most certainly *not* completely sp^2 hybridized but rather something closer to sp^3, since the central carbon has four σ bonds. Although the increasing r_g trend (cf. Table II) implies decreasing s orbital character of the central carbon in going from *t*-BuCl to *t*-BuI, microwave spectroscopic analysis of the three *tert*-butyl halides[32] and force field calculations[33] indicate that the CCX bond angle for all three halides is very close to the tetrahedral value of ~109°. Thus sp^3 hybridization for all three halides should be a good approximation at the reactant equilibrium geometry. In the vicinity of the TS, however, which is our focus, the $G(r, s)$ calculations (cf. section 4) show that the *t*-BuX bond is elongated by ~0.6–0.8 Å over the equilibrium reactant bond length for all halides, implying that the imposed sp^2 hybridization of the central carbon is to some extent a valid approximation for the TS geometry. Perhaps more importantly, even if the changing hybridization were to be accounted for in some way (sp^3 for the reactant geometry, sp^2 for the product, and something intermediate for the TS), we have determined that the numerical differences for complete sp^3 and sp^2 hybridizations in the overlap integrals[31] $S(r)$ result in numerical differences in the properties of the free energy surfaces $G(r, s)$ that are negligible in comparison to their absolute magnitudes. For example, the largest change in $\beta(r^*)$ was found for *t*-BuCl in CH_3CN solvent: $\beta(r^*)(sp^2) \sim 17.7$ kcal/mol; $\beta(r^*)(sp^3) \sim 16.5$ kcal/mol. All other halides in all other solvents had smaller variations in the coupling. This translates into maximum differences in the calculated activation free energies ΔG^* of ~0–0.5 kcal/mol. More importantly, our use of an empirical $E_g(r)$ (cf. eq 3.3) should take the rehybridization effects into account at least partially. (See also the final paragraph of this section.)

Returning to the main theme, the origin of the calculated decreasing *tert*-butyl halide coupling trend is the decreasing energy difference between the diabatic covalent and adiabatic ground states at the reactant geometry (cf. Table II), the ionic-covalent resonance energy (ICRE),[24,25a]

$$\text{ICRE} = D - D_0 \approx \frac{\beta^2(r_g)}{(V_I^0(r_g) - V_C^0(r_g))} = \gamma(r_g)\beta(r_g) \quad (3.6)$$

where the definition of the ionic-covalent mixing coefficient $\gamma(r_g)$ is clear. The diabatic potential gap $V_I^0(r_g) - V_C^0(r_g)$ decreases (cf. Table II) in going from *t*-BuCl to *t*-BuI. However, $\beta(r_g)$ decreases relatively more, so that their ratio $\gamma(r_g)$ actually decreases (cf. Table II); *t*-BuCl has the greatest mixing and *t*-BuI the lowest. The stabilization gained as a result of this mixing, i.e., the ICRE, then decreases.[34,35] The diabatic gap is not as important as the electronic coupling in determining the ICRE.

In summary, the ICREs predict that the C–Cl bond has the highest $\gamma(r_g)$, or the highest *ionic character*, and C–I the lowest. This is the point: we make the quantitative argument that the

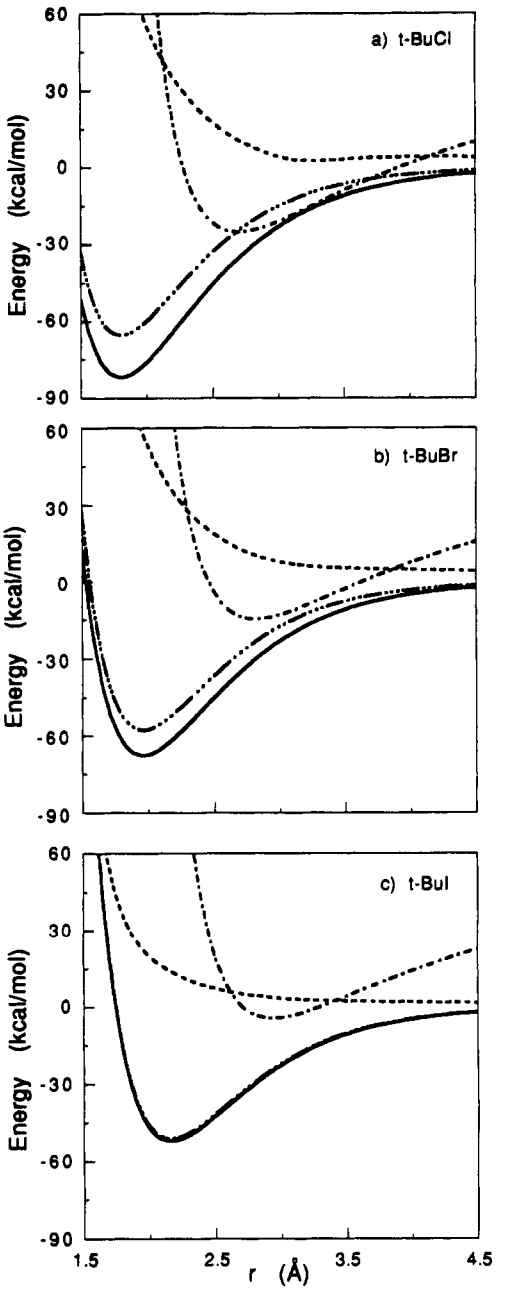

Figure 1. Vacuum Hamiltonians $H^0(r)$ in the orthonormal basis $\{\psi_C, \psi_I\}$ of (a) *t*-BuCl, (b) *t*-BuBr, and (c) *t*-BuI: (—) ground-state $E_g(r)$, (– ··· –) covalent state $V_C^0(r)$, (– · –) ionic state $V_I^0(r)$, and (– –) electronic coupling $\beta(r)$.

(29) Hüttner, W.; Zeil, W. *Spectrochim. Acta* **1966**, *22*, 1007.
(30) $H_{12}^0(r)$ and the overlap $S(r)$ usually have opposite signs. See, e.g.: Newton, M. D. *Int. J. Q. Chem. Symp.* **1980**, *14*, 363.
(31) Mulliken, R. S.; Rieke, C. A.; Orloff, D.; Orloff, H. *J. Chem. Phys.* **1949**, *17*, 1248.
(32) Williams, J. Q.; Gordy, W. *J. Chem. Phys.* **1950**, *18*, 994.
(33) (a) Meyer, A. Y.; Allinger, N. L. *Tetrahedron* **1975**, *31*, 1971. Meyer, A. Y.; Ohmichi, N. *J. Mol. Struct.* **1981**, *73*, 145. Meyer, A. *J. Mol. Struct.* **1983**, *94*, 95.

electronic coupling evaluated at the reactant state directly reflects the ionic character at the reactant state. For any alkyl halide, the coupling will then decrease from the initial reactant value as r increases because the overlap decreases, i.e., the vacuum ionic-covalent mixing decreases.

A supporting argument for this trend can be given by comparing the differences in electronegativities of carbon ($\chi_C = 2.48$) and the three halogens ($\chi_{Cl} = 2.95$, $\chi_{Br} = 2.62$, $\chi_I = 2.52$),[36] which qualitatively measure the bond ionic character;[24] a decreasing reactant ionic character trend is found

$$|\chi_C - \chi_{Cl}| \sim 0.47 \qquad |\chi_C - \chi_{Br}| \sim 0.14 \qquad |\chi_C - \chi_I| \sim 0.04 \quad (3.7)$$

with the C–I bond predicted to be quite covalent in comparison to the other two. On this basis, one could predict that the reactant ionic character, and hence the energy associated with covalent-ionic mixing, should decrease in going from *t*-BuCl to *t*-BuI. This is in agreement with the calculated ICREs, and with Figure 2a. Another straightforward indication of decreasing coupling in the *tert*-butyl halide series is the decreasing BDEs. A reasonable explanation for the trend is that the ionic VB state contributes more for C–Cl than for C–Br and C–I.[37] A greater contribution from the ionic VB state will lower the energy and hence create a stronger bond.[38]

Finally, the approximate wave function forms used to evaluate $S(r)$ have little influence on the coupling behavior described above. Figure 2b shows $S(r)$ for the series, and one can see that the overlap magnitudes evaluated at the respective TSs are approximately the same ($S(r^*) \sim 0.2$). Note that we are not directly calculating the coupling using the appropriate Hamiltonian with the wave functions in eq 3.5 but rather are using model potentials and then evaluating the coupling from them via eq 3.4. In other words, we extract the functional behavior of the coupling which is contained within the vacuum potentials. $G(r, s)$ calculations performed with complete neglect of the overlap results in a maximum difference of ~8% for the computed coupling at the TS for *t*-BuCl and only ~4% for *t*-BuI. The only relation between the coupling and overlap for our vacuum Hamiltonian is that, with increasing r, the overlap should decrease and so should the coupling; there is a greater stabilization associated with covalent-ionic mixing at the respective reactant geometries than at larger separations where there is less mixing.

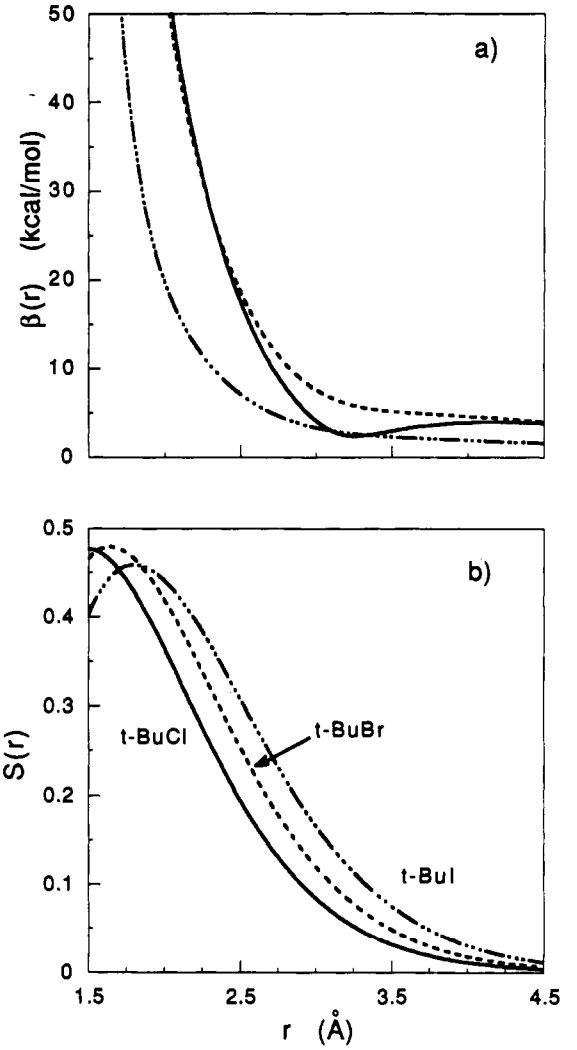

Figure 2. (a) Coupling $\beta(r)$ comparison of *tert*-butyl halides: (—) *t*-BuCl, (– –) *t*-BuBr, and (– ··· –) *t*-BuI. The decreasing trend for $r \leq 3.0$ Å (transition-state vicinities) in going from *t*-BuCl to *t*-BuI is the result of the decreasing energy gap between minima of $E_g(r)$ and $V_C^0(r)$ (ionic–covalent resonance energy). See ref 22. (b) Overlap integrals $S(r)$ of 2p–*Np* carbon–halogen bonds: (—) C–Cl ($N = 3$), (– –) C–Br ($N = 4$), and (– ··· –) C–I ($N = 5$).

4. Model Calculations for Several Solvents

In this section, we present and discuss the alkyl halide $G(r, s)$ surface free energetics and transition-state structure results for a single solvent, CH_3CN, and then as a function of solvent polarity. The electronic polarization response frequency ω_{el} in eq 2.10 (times $\hbar$) is assigned the value of 4.0 eV for all solvents, a characteristic electronic absorption energy for the colorless solvents considered here and in ref 8a.[43]

(34) The approximate formula in eq 3.6 is found to be valid to better than 3.5% for all three *tert*-butyl halides. It is interesting to note that the geometric mean failed for the C–I bond in *t*-BuI until the publication of ref 28a. Only then was the actual bond dissociation energy D for C–I high enough as to not yield a negative ICRE. For example, Ogg and Polanyi[1] reported a C–I BDE of ~44 kcal/mol, while Baughn et al. [Baughn, E. C.; Polanyi, M. *Nature* **1940**, *146*, 685] reported a BDE for C–I of ~46.3 kcal/mol.

(35) In earlier work [Baughn, E. C.; Evans, M. G.; Polanyi, M. *Trans. Faraday Soc.* **1941**, *37*, 337], an experimental dipole moment analysis for C–Cl, C–Br, and C–I was performed in order to determine the validity of Pauling's geometric mean, and it was concluded that the geometric mean *fails* for C–Br and C–I, because the bond ionic character as computed from the ionic dipole moment did not agree with the bond ionic character, $\gamma(r_g)$, as computed from the geometric mean. The entire molecular dipole moment was attributed to the ionic contribution μ_{ion}, which has since been demonstrated in refs 24b, 39, and 41 to be incorrect.

(36) Values are Mulliken–Jaffé electronegativities converted to the Pauling scale. (a) Hinze, J.; Jaffé, H. H. *J. Am. Chem. Soc.* **1962**, *84*, 540. (b) *J. Phys. Chem.* **1963**, *67*, 1501. (c) *J. Am. Chem. Soc.* **1963**, *85*, 148.

(37) C and Cl bonding orbitals may be more closely matched in size than for either Br or I, which would yield better overlap and hence a stronger bond. However, the Slater 2*p* and *Np* ($N = 3, 4, 5$) orbitals discussed in section 3A give approximately the same numerical value for the overlap (~0.41) at the respective reactant geometries.

(38) Experimentally determined molecular dipole moments can also give measures of ionic character[39-41] and thus might provide another approach to establishing the electronic coupling trend. Caution must be used, however, in directly attributing the entire molecular moment $\bar{\mu}$ to the ionic character. The ionic bond moment can be only one of several contributions to $\bar{\mu}$.[24b,39,41] Two other contributions are the moments arising from atomic size differences (homopolar dipole moment) and from the electronic hybridization, including the polarization of nonbonding electrons. For bonds between atoms of not too disparate size, dipole moments associated with the atom hybridizations are larger than homopolar moments and sometimes can account for most of the experimentally observed $\bar{\mu}$.[42] The experimental $\bar{\mu}$'s, as determined via the microwave Stark effect, for the *tert*-butyl halides are[40] (in Debye) $|\mu_{exp}^{Cl}| = 2.15$, $|\mu_{exp}^{Br}| = 2.21$, and $|\mu_{exp}^{I}| = 2.13$ D. If one could assign some constant percentage of these values to the ionic bond moment, they would indicate that the ionic character of the C–X bonds *does* decrease, since the equilibrium bond length r_g increases in going from *t*-BuCl to *t*-BuI (cf. Table II).

(39) See, e.g.: Gordy, W. *Faraday Disc. Chem. Soc.* **1955**, *19*, 14.

(40) Townes, C. H.; Schawlow, A. L. *Microwave Spectroscopy*; McGraw-Hill: New York, 1955.

(41) (a) Minkin, V. I.; Osipov, O. A.; Zhdanov, Y. A. *Dipole Moments in Organic Chemistry*; Plenum: New York, 1970. (b) Ruedenberg, K. *Rev. Mod. Phys.* **1962**, *34*, 362. (c) Gibbs, J. H. *J. Phys. Chem.* **1955**, *59*, 644. (d) Coulson, C. A. *Trans. Faraday Soc.* **1942**, *38*, 433. (e) Robinson, D. Z. *J. Chem. Phys.* **1949**, *17*, 1022. (f) Burnelle, L.; Coulson, C. A. *Trans. Faraday Soc.* **1957**, *53*, 403. (g) Coppens, P.; Hirshfield, F. L. *Isr. J. Chem.* **1964**, *2*, 117. (h) Duncan, A. B. F.; Pople, J. A. *Trans. Faraday Soc.* **1953**, *49*, 217.

(42) See ref 27b, p 161 for an example of NF_3 and NH_3.

A. Free Energy Surfaces and TS Character. The fixed solvent polarity *tert*-butyl halide trends in this subsection refer to the order Cl, Br, and I. As an initial example of these trends, calculated free energy surface contours are shown in Figure 3a–c for the polar solvent acetonitrile CH_3CN ($\epsilon_0 \sim 36.0$, $\epsilon_\infty \sim 1.8$).[44] The conditions

$$\frac{\partial G(r, s)}{\partial r} = \frac{\partial G(r, s)}{\partial s} = 0 \qquad (4.1)$$

determine the surface extrema. The reactant state corresponds to the local minimum in the lower left hand corner and the TS corresponds to the saddle point. Both extrema are equilibrium solvation states, since both solvent polarizations $\vec{P}_{el}$ and $\vec{P}_{or}$ are equilibrated to the solute charge distribution. For now, the product "state" is identified as the exit channel located at $r \sim 3.0$–3.5 Å and $s_{eq} = c_I^{2eq} \approx 1$ (100% ionic character). The steepest descent, solution reaction path[8b,12,45] free energy projections onto r in going from reactants to products are displayed in Figure 4 for the *tert*-butyl halide series, corresponding to the free energy contours in Figure 3a–c.

For the *t*-BuX reactant states in CH_3CN, the ionic characters c_I^{2eq} are quite small and decrease [$c_I^{2eq} \sim 0.03, \sim 0.02, \sim 0.01$], and the equilibrium bond lengths in solution r_{eq} are essentially the same as the vacuum values. Since the reactant states in solution do not differ greatly from the vacuum, the respective reactant free energies G_R^{eq} and locations should be nearly the same as the (negative) adiabatic ground state BDEs, and indeed this is the case.[46]

Table III lists the TS locations in CH_3CN: the *tert*-butyl halides exhibit the trends of increasing absolute C–X separation and decreasing ionic character at the TS for fixed solvent polarity. Since the ionic character decreases, the solvent stabilization at the TS $\Delta G_{\ddagger,solv}^{eq}$, also displayed in Table III and given by (cf. eq 2.7),

$$\Delta G_{\ddagger,solv}^{eq} = -(\Delta G_r c_I^{2\ddagger} + \Delta G_r^{el}) c_I^{2\ddagger} + \frac{1}{4}\Delta G_r^{el} y^{2\ddagger} f^{\ddagger} \qquad (4.2)$$

also decreases (i.e., $\Delta G_{\ddagger,solv}^{eq}$ becomes less negative). It is important to emphasize the relation between TS ionic character and solvent stabilization: a less polar solute will result in less solvent stabilization due to smaller solvent–solute electrostatic interactions.

The observed increasing absolute TS separation trend is to be expected, given the increasing reactant separations r_{eq} and decreasing BDEs. However one might expect at first glance a larger separation to have a greater ionic character. This suggests examination of the net change, $\Delta r^{\ddagger} = r^{\ddagger} - r_{eq}$, as a possible measuring of effective separation at the TS. One find $\Delta r_{Cl}^{\ddagger} = 0.69$, $\Delta r_{Br}^{\ddagger} = 0.69$, $\Delta r_I^{\ddagger} = 0.67$ Å, which does not give any more clarification, since C–Cl and C–Br would have the same ionic character if this approach were valid. What is necessary then is to evaluate a (dimensionless) *relative* change of the TS separation compared to the reactant. To this end, we introduce the relative separation $\Delta\bar{r}^{\ddagger}$ at the TS

$$\Delta\bar{r}^{\ddagger} \equiv \frac{\Delta r}{r_{eq}} = \frac{r^{\ddagger} - r_{eq}}{r_{eq}} \qquad (4.3)$$

which is simply the net percent change in C–X separation at the TS compared to the reactant. Evaluation gives $\Delta\bar{r}_{Cl}^{\ddagger} = 0.38$, $\Delta\bar{r}_{Br}^{\ddagger} = 0.35$, $\Delta\bar{r}_I^{\ddagger} = 0.31$. Thus, *t*-BuCl requires the largest relative bond elongation in order to reach the TS, and *t*-BuI the smallest. This relative $\Delta\bar{r}^{\ddagger}$ scale is evidently the correct way to assess the TS separation as it agrees with the decreasing TS ionic character trend (cf. Table III).

Table III lists the TS free energies $G^{\ddagger}$. The observed increasing trend is to be expected, given that the reactant BDEs and halogen electron affinities (EA) decrease (cf. Tables I and II). In addition, the magnitude of $\Delta G_{\ddagger,solv}^{eq}$ also decreases, which combines with the BDE and EA trends to further establish the order of $G^{\ddagger}$ for the series. However, the decreasing electronic coupling trend, which stabilizes[1,8a] the TS via the $-\beta(r)y$ term in eq. 2.7, also contributes significantly to the $G^{\ddagger}$ trend. The computed coupling values, given in Table III, are the approximate magnitudes of the coupling stabilizations since $y^{\ddagger} = 2c_C^{\ddagger}c_I^{\ddagger} \approx 1$ for all halides. Combining these with the $\Delta G_{\ddagger,solv}^{eq}$ values, the coupling accounts for $\sim$65%, $\sim$60%, and $\sim$35% of the total TS stabilization for the series. As explained in section 3B, the decreasing coupling $\beta(r^{\ddagger})$ trend is ultimately a reflection of the decreasing ICREs at the reactant stage.

The calculated activation free energies $\Delta G^{\ddagger}$ are also given in Table III, and all are in good agreement with experiment[3] (cf. Figure 9a). Notice that the $\Delta G^{\ddagger}$ trend is opposite to the TS free energy ($G^{\ddagger}$) trend, i.e., *t*-BuI has the highest $G^{\ddagger}$ but the lowest $\Delta G^{\ddagger}$. Traditionally,[1] the explanation for this would be based on the BDEs, as follows. *t*-BuCl has the highest BDE, and therefore a larger energy would be required to break the C–Cl bond; hence a higher activation free energy would be required for ionization. Accordingly, *t*-BuBr would be intermediate, and *t*-BuI the lowest. Our results indicate that the $\Delta G^{\ddagger}$ trend requires much closer scrutiny. First, it is not the differences of the BDEs themselves that are relevant, but rather it is the relative difference in the BDE change compared to the halogen EA change. For if the ionic state moves up in energy the same amount that the BDE decreases, little or no change in $\Delta G^{\ddagger}$ would be expected. With the data in Tables I and II, the net difference in BDEs and EAs is $\sim$16.9 kcal/mol, which is $\sim$11.2 kcal/mol *greater* than the calculated difference in $\Delta G^{\ddagger}$ of $\sim$5.7 kcal/mol (cf. Table III). The second consideration must then be the electronic coupling trend, which stabilizes the TS as discussed above. Indeed, inspection of the data in Table III shows that the much greater coupling for *t*-BuCl compared to *t*-BuI accounts for the $\sim$11.2 kcal/mol discrepancy. Note that the TS stabilization due to $\Delta G_{\ddagger,solv}^{eq}$, although slightly greater for *t*-BuCl than for *t*-BuI, cannot alone overcome the BDE–EA relative difference and plays a relatively minor role in establishing the $\Delta G^{\ddagger}$ trend. In summary, the *tert*-butyl halide $\Delta G^{\ddagger}$ trend can be understood by consideration of the relative BDE–EA difference *and* the difference in TS electronic coupling stabilization. The individual contributions to $\Delta G^{\ddagger}$ are discussed in more detail in section 5.

The net picture at this point is that the "lateness" of the TS, i.e., separation and ionic character, decreases for *t*-BuX ionization for the series in a given solvent. The solvent stabilization at the TS also decreases, which is a direct consequence of the decreasing ionic character, as does the activation free energy. If as in 1 we appeal to the Hammond postulate,[47–49] the TS lateness trend should be correlated with the various ΔG_{rxn} values, where ΔG_{rxn} is the free energy difference of the product and reactant locations, and we now examine this. Since the exit channels in Figure 3a–c continuously decrease, there is no well-defined product well, so ΔG_{rxn} is evaluated at $\sim$1 Å greater than the respective $r^{\ddagger}$ values (cf. Table III). Evaluation gives $\Delta G_{rxn} = 11.6$, 9.3, and 8.1 kcal/mol; the ionization becomes less endothermic, or equivalently the product ion pair becomes more stabilized relative to the reactant. Relative increase of product stabilization should mean that the TS becomes more reactant-like; our predicted TS relative separation and ionic character trends thus are consistent with the

(43) This is approximately a UV absorption energy for the solvents studied here. Grasselli, J. G.; Ritchey, W. M. *Atlas of Spectral Data and Physical Constants for Organic Compounds*; CRC: Cleveland, 1975.

(44) Reichardt, C. *Solvents and Solvent Effects in Organic Chemistry*, 2nd ed.; VCH Verlagsgesellschaft mbH: Weinheim, 1988.

(45) (a) Fukui, K. *J. Phys. Chem.* **1970**, *23*, 4161; *Acc. Chem. Res.* **1981**, *14*, 363. (b) Lee, S.; Hynes, J. T. *J. Chem. Phys.* **1988**, *88*, 6863.

(46) The solvent well along s at the respective r_{eq} values is very broad due to the small solvent force constant ($\sim 2\Delta G_r$) there. However, the solvent well frequencies ω_s^0, and the corresponding solvent well entropic effect (via $-k_B T \ln[k_b T/\hbar\omega_s^0]$), at the reactant and product ($r \sim 3.5$ Å) locations are the same due to the nonchanging charge distributions in these local regions.[8b,12]

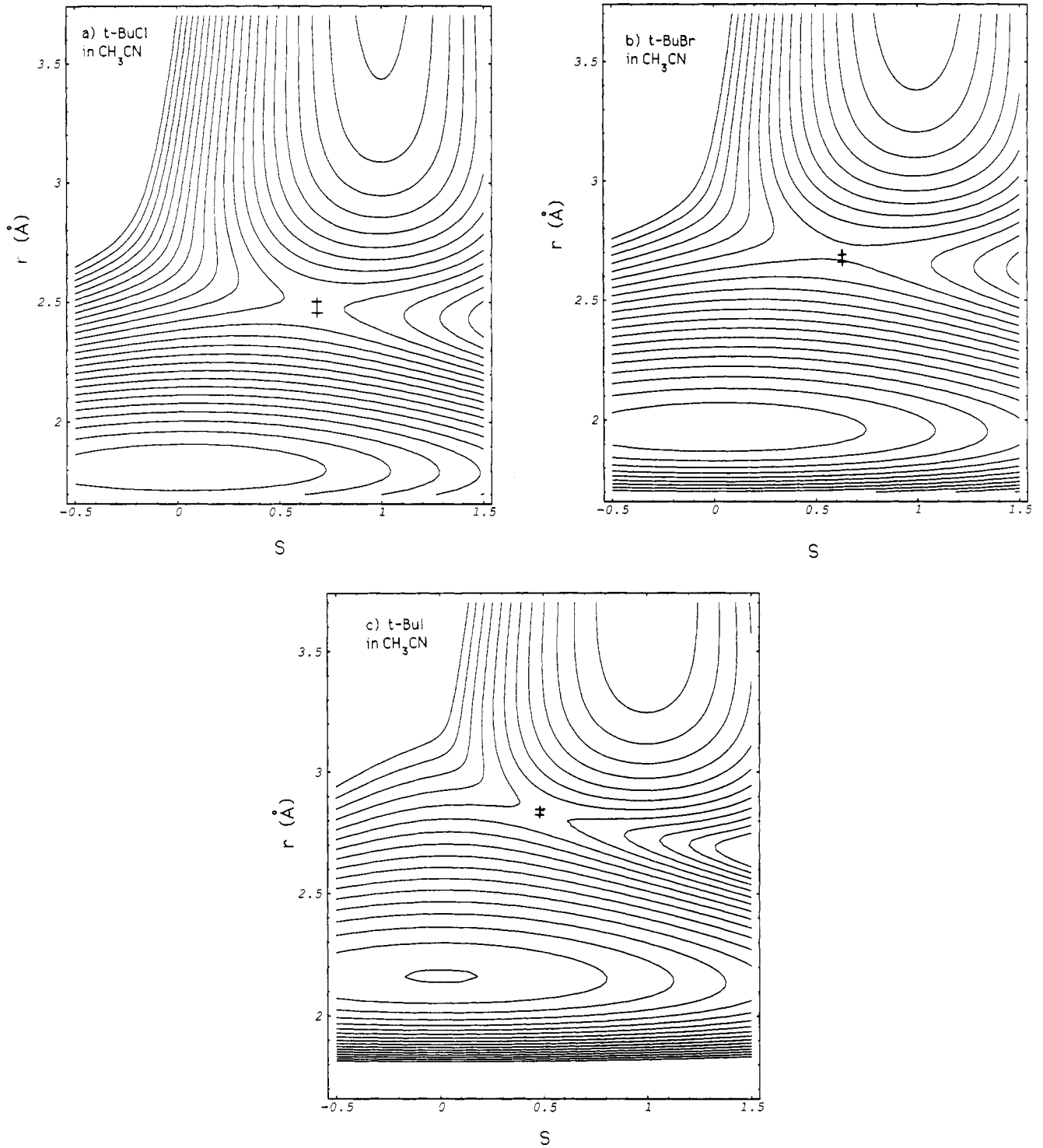

Figure 3. Free energy contour surfaces for ionization in CH_3CN solvent: (a) *t*-BuCl, (b) *t*-BuBr, and (c) *t*-BuI. Contour lines are 2.0 kcal apart. The displayed coordinates are not mass-weighted.[12]

Hammond postulate.[47-49] But *why* the halides exhibit these trends has not yet been addressed. In section 5A, it will be demonstrated and explained that the decreasing TS ionic character trend is the result of the *decreasing variation with r in the electronic coupling* $\beta(r)$.[50]

The leaving group ability, as determined by the relative basicities of the free ions,[49] increases according to $Cl^- < Br^- < I^-$. The data in Table III show that relative TS bond extension, $\Delta\bar{r}^{\ddagger}$, is a good parameter to reflect this ability: a better leaving group requires a smaller bond extension. By contrast, TS solvent stabilization is not a good indicator, as the best leaving group receives the smallest stabilization. Again, these observations are consistent with Hammond postulate behavior,[47-49] in that a more stabilized product has a more reactant-like TS in both charge distribution and geometry.

Figure 5a displays a Brønsted plot,[51] $\Delta G^{\ddagger}$ vs ΔG_{rxn}, for the series in CH_3CN. The slope $\beta_B = d\Delta G^{\ddagger}/d\Delta G_{rxn}$ in Figure 5a, commonly associated with reflecting TS ionic character,[52,53] is not constant and is correlated with the TS ionic character in Figure 5b. A larger β_B correlates with a larger $c_I^{2\ddagger}$, again in

(47) Hammond, G. S. *J. Am. Chem. Soc.* **1955**, *77*, 334.
(48) Bell, R. P. *Proc. Roy. Soc. (London)* **1936**, *A154*, 414. Evans, M. G.; Polanyi, M. *Trans. Faraday Soc.* **1938**, *34*, 11.
(49) See, e.g.; Lowry, T. H.; Richardson, K. S. *Mechanism and Theory in Organic Chemistry*; 3rd ed.; Harper and Row: New York, 1987.

Table III. Calculated Transition-State Quantities for *tert*-Butyl Halide S_N1 Ionization in CH_3CN

	t-BuCl	*t*-BuBr	*t*-BuI
$r^{\ddagger}$ (Å)	2.49	2.65	2.83
$c_I^{2\ddagger}$	0.66	0.60	0.49
$\Delta r^{\ddagger}$	0.38	0.35	0.31
$G^{\ddagger}$ (kcal/mol)	−52.3	−42.2	−28.2
$\Delta G^{\ddagger}$ (kcal/mol)	29.5	25.5	23.8
$\Delta G^{eq}_{s,solv}$ (kcal/mol)	−9.8	−8.8	−7.9
$-\beta(r^{\ddagger})$ (kcal/mol)	−17.7	−13.9	−4.1

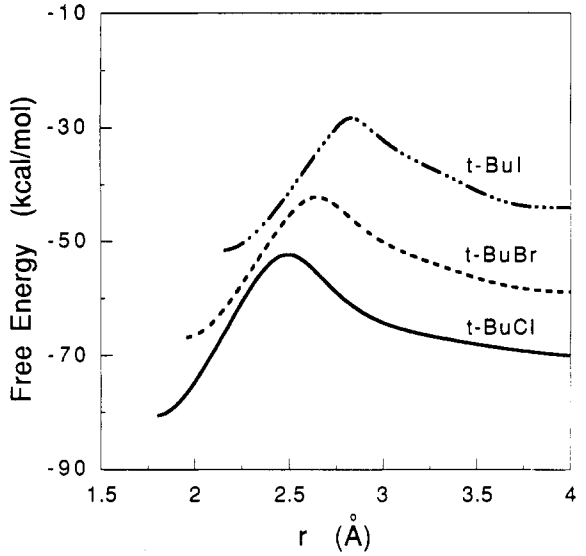

Figure 4. Free energies projected onto r along the solution reaction path[8b,12,45] for ionization in acetonitrile: (—) *t*-BuCl, (– –) *t*-BuBr, and (– ··· –) *t*-BuI.

agreement with the Hammond postulate.[47-49] It is also worth noting that the slope β_B in Figure 5a is greater than unity. This is of interest in that the usual explanations[54] for such behavior, e.g., a change in reaction mechanism, are absent in the present model. Other than the trivial relation $\delta\Delta G^{\ddagger} > \delta\Delta G_{rxn}$, or equivalently $\delta G^{\ddagger} < \delta G_P$ where G_P is the product free energy, we have been unable to derive a more useful analytic formula for β_B to clarify the origin of the $\beta_B > 1$ behavior.[55]

Finally, Figure 6a–c displays projections of the free energy surfaces at the respective fixed $r^{\ddagger}$ values along the solvent coordinate s for CH_3CN solvent. For *t*-BuCl and *t*-BuBr there is a single solvent well; the free energy is minimum when the solvent is equilibrated to the existing ionic character. As

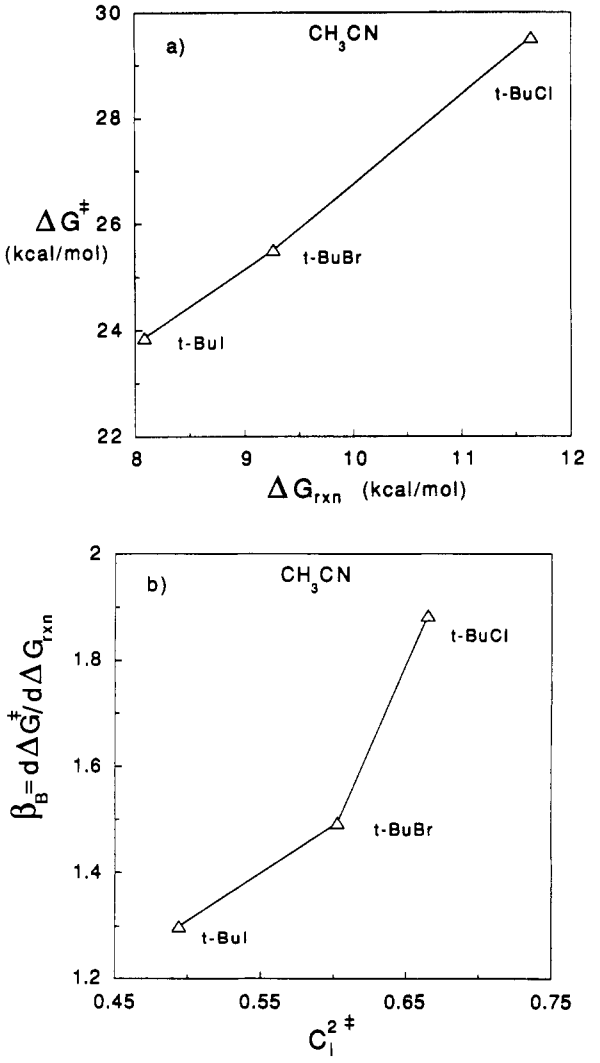

Figure 5. (a) Brønsted plot for the *tert*-butyl halide series in acetonitrile and (b) correlation of the slope β_B in (a) with the transition-state ionic character. The data points correspond to calculated quantities for *t*-BuI, *t*-BuBr, and *t*-BuCl, respectively.

emphasized in 1, the single well character guarantees that the ionization has no activated electron-transfer character. But for *t*-BuI there is a barrier in the solvent coordinate of ~0.9 kcal/mol, which is ~4% of the total calculated activation free energy. The solvent barrier can also be recognized in Figure 3c by the larger angle relative to the s axis of the solvent well in the saddle point region. Whether or not a solvent barrier is present for any charge-transfer system depends on the magnitudes of the coupling compared to the solvation when both are evaluated at the TS. As explained in detail in ref 9, the correct condition for a solvent barrier is approximately $2\beta/\Delta G_r < 1$.[56,57] The TS quantities for *t*-BuI in CH_3CN are $\Delta G_r(r^{\ddagger}) = 15.5$ and $\beta(r^{\ddagger}) = 4.1$ kcal/mol,

(50) Abraham has postulated that the lateness of the TS decreases in going from *t*-BuCl to *t*-BuI, assuming that the TS solvent stabilization is directly proportional to the ionic character ($c_I^{2\ddagger}$). We have found a decreasing $c_I^{2\ddagger}$ trend, in qualitative agreement with Abraham, although it has been shown in 1 and again here in eq 5.9 that the TS solvent stabilization is instead proportional to the *square* of the ionic character. More importantly, our reasoning why the lateness trend is observed differs fundamentally from Abraham's (cf. section 5A). (a) Abraham, M. H.; Johnston, G. F. *J. Chem. Soc. A* **1971**, 1610. (b) Abraham, M. H. *Prog. Phys. Org. Chem.* **1974**, *11*, 1. (c) Abraham, M. H.; Taft, R. W.; Kamlet, M. J. *J. Org. Chem.* **1981**, *46*, 3053.

(51) Brønsted. J. N.; Pederson, K. *Z. Phys. Chem.* **1924**, *108*, 185.

(52) (a) Leffler, J. E. *Science* **1953**, *117*, 340. (b) Lewis, E. S. In *Techniques of Chemistry*; Bernasconi, C. F., Ed.; Wiley and Sons: New York, 1986; Vol. 6, Part 1. (c) Lewis, E. S. *J. Phys. Org. Chem.* **1990**, *3*, 1. See also ref 54 for examples where a Brønsted slope could not be interpreted as measuring the TS ionic character.

(53) (a) Rao, S. N.; More O'Ferrall, R. A. *J. Am. Chem. Soc.* **1990**, *112*, 2729. (b) Bernasconi, C. F.; Killion, R. B., Jr. *J. Org. Chem.* **1989**, *54*, 2878. (c) Bernasconi, C. F.; Leonarduzzi, G. D. *J. Am. Chem. Soc.* **1982**, *104*, 5133. (d) Lewis, E. S.; More O'Ferrall, R. A. *J. Chem. Soc., Perkin Trans. II* **1981**, 1084. (e) Grunwald, E.; Leffler, J. E. *Rates and Equilibrium in Organic Reactions*; Wiley: New York, 1964.

(54) See, e.g.: Bordwell, F. G.; Hughes, D. L. *J. Am. Chem. Soc.* **1985**, *107*, 4737. Gilbert, H. F.; Jencks, W. P. *J. Am. Chem. Soc.* **1979**, *101*, 5774. Bordwell, F. G.; Branca, J. C.; Cripe, T. A. *Isr. J. Chem.* **1985**, *26*, 357.

(55) Evaluation of ΔG_{rxn} at several other reasonable product locations all give $\beta_B > 1$. Product definitions other than that (a) in text ($r \approx 3.5$ Å) include (b) simple multiples of $\Delta r^{\ddagger}$, (c) constant $\Delta r \geq 1$ (cf. section 5C), (d) the 100% ionic character location in r along the paths in Figure 4, and (e) infinite ($r \rightarrow \infty$) nuclear separation. It is found, however, that the correlation of β_B with $c_I^{2\ddagger}$ can depend on where ΔG_{rxn} is evaluated. Positive correlations like that in Figure 5b result when ΔG_{rxn} is evaluated near $r \lesssim r^{\ddagger} + 1.5$ Å, a value characteristic of nuclear separations for solvent separated ion pairs. When evaluated at large separations ($r > r^{\ddagger} + 1.5$ Å; cases (c)–(e) above), negative correlations between β_B and $c_I^{2\ddagger}$ are found (a larger β_B has a *smaller* $c_I^{2\ddagger}$). This inverse correlation results from a smaller ΔG_{rxn} difference between "product" *t*-BuI and *t*-BuBr than their $\Delta G^{\ddagger}$ difference at such larger distances. See [Marcus, Y. *Ion Solvation*; Wiley: New York, 1985] for X^- solvation free energies in CH_3CN.

(56) Mathis, J. R.; Kim, H. J.; Hynes, J. T. *Solvent Barriers in Unimolecular Ionizations: S_N1 Ionization of Alkyl Iodides*; to be submitted.

so $2\beta(r^{\ddagger})/\Delta G_r(r^{\ddagger}) \approx 0.5$ (the ratio is greater than unity for *t*-BuCl and *t*-BuBr). The relatively weak electronic coupling and consequent presence of a solvent barrier for the model *t*-BuI system is ultimately a reflection of a primarily covalent reactant state, i.e., little or no ionic mixing there (cf. section 3B).[58] But in any event, as the results within demonstrate, there is no explicit TS trend signature for *t*-BuI that is different from the trends for *t*-BuCl and *t*-BuBr. The origins and implications of a solvent barrier in unimolecular ionizations, in particular regarding a possible electron-transfer mechanism suggested in Figure 6c, will be addressed elsewhere.[56]

B. Solvent Polarity Trends. Passing now to solvent polarity trends, we consider the TS behavior of the *t*-BuX ionization in four model aprotic solvents spanning a large range of polarity. In order of increasing polarity these are chlorobenzene C_6H_5Cl ($\epsilon_0 \sim 5.6$, $\epsilon_\infty \sim 2.3$), dichloromethane CH_2Cl_2 ($\epsilon_0 \sim 8.9$, $\epsilon_\infty \sim 2.0$), acetone $(CH_3)_2CO$ ($\epsilon_0 \sim 20.6$, $\epsilon_\infty \sim 1.9$),[44] and CH_3CN. (If Z or E_T are used to measure solvent polarity, the solvent order is the same.[50a]) Now the terms increasing and decreasing will refer to the behavior of the individual *t*-BuX species as the solvent polarity is increased, in contrast to the fixed polarity usage of these terms in section 4A.

Displayed in Figure 7a,b are plots of the TS separation $r^{\ddagger}$ and ionic character $c_I^{2\ddagger}$ versus the Pekar[59] factor

$$C \equiv \frac{1}{\epsilon_\infty} - \frac{1}{\epsilon_0} \tag{4.4}$$

which serves as a convenient measure of solvent polarity.[8] As in the initial *t*-BuCl ionization analysis in 1, the TS locations for all three *tert*-butyl halides move toward the reactants in both r and s. *All the TSs become tighter and less ionic with increasing solvent polarity*, in direct contrast to many statements in the literature.[3-5] The net $r^{\ddagger}$ and $c_I^{2\ddagger}$ changes are all similar for the three halides, especially if $\Delta\bar{r}^{\ddagger}$ is used to measure the relative separation at the TS instead of $r^{\ddagger}$. Indeed, a striking linear correlation of TS ionic character and relative TS separation is provided by Figure 8.[60] This demonstrates that a strong correlation (approximately linear) between the relative TS separation and the TS ionic character exists,[61] which is at variance with suggestions in the literature for other systems.[62]

In Figure 9a, the calculated activation free energies $\Delta G^{\ddagger}$ for ionization are compared with the experimental values.[3] The calculated $\Delta G^{\ddagger}$ values for all *tert*-butyl halides agree with these to within 1.5 kcal/mol, which is quite remarkable given the simplicity of our vacuum potentials and solvent model. Note the trend of decreasing $\Delta G^{\ddagger}$, and hence increasing reaction rate, for all three halides. The traditional Hughes–Ingold[2-5] explanation of this trend is that an ionic TS is stabilized to a greater extent in a highly polar solvent as compared to a weakly polar solvent: an increase in solvent stabilization is supposed to result in a decrease in the reaction barrier, hence an increase in the reaction rate. However, it has been shown in 1 and in this work (cf. Figure 7b) that the ionic characters of the TSs actually decrease; thus the magnitude of the solvation at the TSs should also *decrease*. (Recall from section 4A that in a fixed solvent, decreasing TS ionic characters for the series also gave a decreasing TS solvation magnitude.) Figure 9b shows the calculated TS solvation free energies, and indeed the solvation at the TSs does decrease; the TS is actually *less* stabilized in a high polarity solvent (CH_3CN) compared to a weak polarity solvent (C_6H_5Cl). This result is of paramount importance, as it is in stark contrast with the conventional[2-5] explanation for increasing rates of unimolecular ionizations for greater solvent polarity.

Figure 10a shows individual Brønsted plots[51] for the three halides with varying solvent polarity, i.e., $\Delta G^{\ddagger}$ vs the reaction free energy ΔG_{rxn} for a given species. As in Figure 5a for the series in a fixed solvent, the slope in Figure 10a for the individual halides, denoted by α, is not constant, an effect more clearly seen in Figure 10b. In the case of *t*-BuI, for example, it varies by about a factor of 2 ($\sim$0.05 in CH_3CN to $\sim$0.12 in C_6H_5Cl). As mentioned previously, it is common practice to associate the slope of a structure–reactivity relationship,[52,53] such as in Figure 10a, with the TS ionic character. Our calculated results in fact agree with this analogy. Figure 10c illustrates the correlation of α with $c_I^{2\ddagger}$, where smaller α's denote more reactant-like TSs in highly polar solvents, and larger α's denote more product-like TSs in weakly polar solvents (but identification of the numerical value of α as equal to the TS ionic character is not correct[8a]). This variation of α is thus an explicit signature of an earlier TS with increasing solvent polarity,[8a] as Figure 10b shows. Further discussion of α and its relation to $c_I^{2\ddagger}$ will be given in section 5C.[63]

Finally, rate constants k are calculated for the *tert*-butyl halides using the solution reaction path[8b,12,45] (SRP) according to the methods described in ref 8b. Even though there is a solvent barrier present for *t*-BuI, which suggests a possible electron-transfer mechanism, a rate constant analysis[56] in fact shows that an electron-transfer perspective is *not* correct and that the best estimate to the actual rate constant is one using the SRP. Further details regarding the influence of a solvent barrier in unimolecular ionizations are found in ref 56. The transition-state theory rate constant k using the SRP (cf. Figure 4) is given by[8b,12,45]

$$k = \frac{k_B T Q_\perp^{\ddagger}}{h\ Q_R} \exp[-G^{\ddagger}/k_B T] = \frac{\omega_s^0\, \omega_R}{2\pi\omega_\perp} \exp[-\Delta G^{\ddagger}/k_B T] \tag{4.5}$$

where $Q_\perp^{\ddagger}$ is the partition function for the transverse normal mode at the TS,[12] and $\omega_\perp$ is the corresponding classical frequency. Q_R is the reactant partition function, classical evaluation of which gives the reactant solvent well[8b,12] and reactant vibrational frequencies ω_s^0 and ω_R, respectively,[64] and $\hbar$ is Planck's constant. Table IV displays the results, as $-\log k$, and the experimental values[3] for the solvents listed above. The main source of the disagreement between the calculated and experimental values is $\Delta G^{\ddagger}$. However, as was discussed in ref 8b, experimental definition of $\Delta G^{\ddagger}$ is somewhat ambiguous, and differences of $\sim$1 kcal/mol are to be expected.

5. Transition-State Trend Analysis

In this section, we analyze in greater detail the major results of the previous section. Specifically, we examine the conditions that determine the TS *location* and use them to explain the *t*-BuX TS trends for a fixed solvent (cf. section 4A and Table III). The

(57) In the self-consistent limit ($f \to \infty$), this ratio is $2\beta/(\Delta G_r + \Delta G_r^{el})$. See refs 9a and 20.

(58) One might therefore expect other systems with very covalent reactant bonds, e.g., carbon–sulfur bonds with their small electronegativity difference ($|\chi_C - \chi_S| \sim 0.1$),[36] to exhibit a solvent barrier in the TS vicinity. However, one must also consider product stability and consequently whether or not a unimolecular reaction mechanism is likely. For carbon–sulfur bonds, the sulfide anion is a weak base, but much stronger than halogen anions, and as much is not as good a leaving group as is I^-,[49] thus the bond breakage may require a bimolecular mechanism.[49]

(59) Pekar, S. I. *Untersuchungen über die Elektronentheorie der Kristalle*; Akadamie-Verlag: Berlin, 1954.

(60) We have investigated this for the isopropyl iodide parameter set described in ref 56, and it also exhibits a linear correlation of TS relative separation and TS ionic character.

(61) Mathis, J. R. Ph.D. Thesis, University of Colorado, unpublished.

(62) Pross, A. *Adv. Phys. Org. Chem.* **1985**, *21*, 99.

(63) In contrast to the remark in ref 55, α always correlates positively with $c_I^{2\ddagger}$, regardless of where ΔG_{rxn} is evaluated. The reason is that the product free energy for a given *tert*-butyl halide continuously decreases as solvent polarity is increased.

(64) Values of ω_R used are 107.4, 97.9, and 92.7 ps^{-1} for *t*-BuCl, *t*-BuBr, and *t*-BuI, respectively [Dollish, F. R.; Fateley, W. G.; Bentley, F. F. *Characteristic Raman Frequencies of Organic Compounds*; Wiley: New York, 1974]. Reactant solvent well frequency ω_s^0 in all solvents is given the value 8.3 ps^{-1} [Maroncelli, M. *J. Chem. Phys.* **1991**, *94*, 2084], while the computed values of $\omega_\perp$ are 8.4, 8.5, and 8.8 ps^{-1} (all are relatively polarity independent[8b]). Thus, the computed prefactors to the exponential in eq 4.5 are $\sim 4.8 \times 10^{13}$, $\sim 1.5 \times 10^{13}$, and $\sim 1.4 \times 10^{13}$ s^{-1} for *t*-BuCl, *t*-BuBr, and *t*-BuI, respectively.

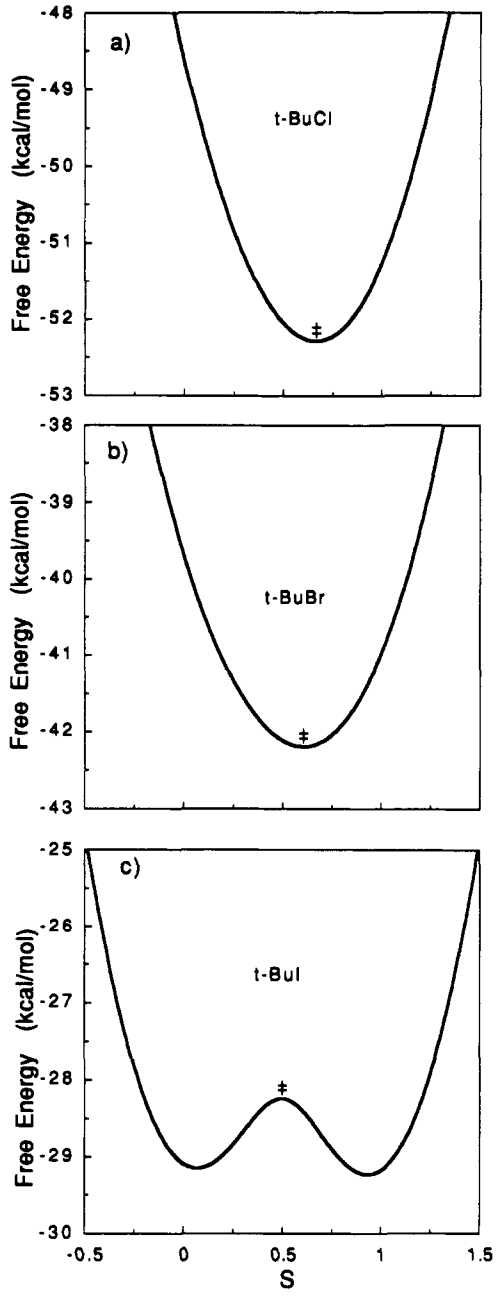

Figure 6. Free energy profiles in CH_3CN solvent along the solvent coordinate s at the respective transition-state separation $r^\ddagger$ values: (a) t-BuCl, (b) t-BuBr, and (c) t-BuI. For t-BuI, the electronic coupling compared to the solvation at the transition state is weak enough to cause a barrier in the solvent coordinate. As noted in text, the existence of a solvent barrier for t-BuI, which according to calculations is present in all solvents studied, has no effect on the TS polarity trends.[56]

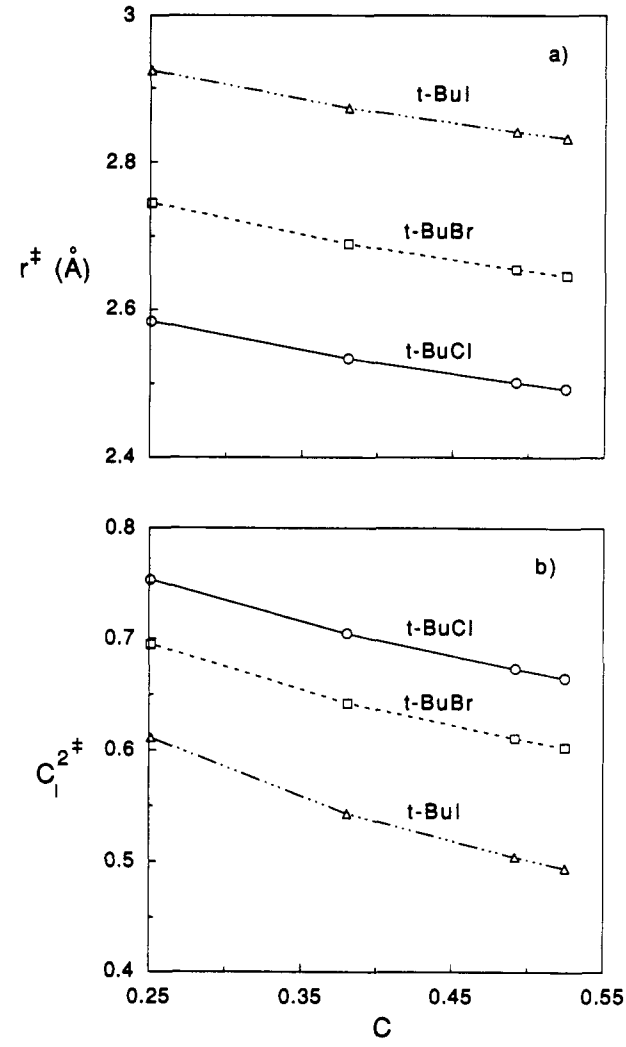

Figure 7. The *tert*-butyl halide transition-state structure variation with polarity factor $C \equiv \epsilon_\infty^{-1} - \epsilon_0^{-1}$: (a) transition-state separation $r^\ddagger$ and (b) ionic character $c_I^{2\ddagger}$. The data points correspond to the calculated values for ionization in C_6H_5Cl, CH_2Cl_2, $(CH_3)_2CO$, and CH_3CN solvents.

novel $c_I^{2\ddagger}$ and $r^\ddagger$ trends (cf. Figure 7) with increasing solvent polarity have been examined in detail in 1; therefore their analyses will not be repeated here. Simply stated, both $c_I^{2\ddagger}$ and $r^\ddagger$ polarity trends are examples of Hammond postulate[47-49] behavior, where increasing product stability moves the TS toward the reactants, in this case in both r and s (cf. eq 2.14). We also examine here the activation barrier *origin* for the *tert*-butyl halides, since the TS solvent stabilization decreases with increasing polarity for all of them (cf. Figure 9b), in contrast to the Hughes–Ingold perspective.[2-5] In addition, the correlation between the TS ionic character and the slope α of the Brønsted plot series (cf. Figure 10) will be analyzed.

A. TS Ionic Character. The TS analysis starts by determining the TS condition. By differentiating eqs 2.7 and 2.12 and combining with eq 2.14, one obtains

$$\left.\frac{\partial G}{\partial r}\right|_\ddagger \approx V_C^{0\prime}(r^\ddagger)c_C^{2\ddagger} + V_I^{0\prime}(r^\ddagger)c_I^{2\ddagger} - 2\beta'(r^\ddagger)c_I^\ddagger c_C^\ddagger \quad (5.1)$$

$$- \Delta G'_r(r^\ddagger)c_I^{2\ddagger} - \Delta G'_{el}(r^\ddagger)((1-f^\ddagger) + c_I^{2\ddagger}f^\ddagger) = 0$$

where the $'$ denotes an ordinary r derivative. Equation 5.1 is the same as eq A.1 in 1, but with the further approximations that $\Delta G_{el}(r^\ddagger)/2\hbar\omega_{el} \approx 0$ and that the r dependence of the centrifugal temperature term in eq 2.7 is negligible in comparison to the quantities displayed. Both approximations can safely be made[65] and simplify the analysis. Equation 5.1 can be rearranged to yield the very instructive relation

$$-[F_C(r^\ddagger) + 2\sqrt{K^\ddagger}\beta'(r^\ddagger)] = K^\ddagger F_{I,eff}(r^\ddagger) \quad (5.2)$$

where

$$F_{I,eff}(r^\ddagger) \equiv -(V_I^{0\prime}(r^\ddagger) - \Delta G'_r(r^\ddagger)c_I^{2\ddagger} - \Delta G_r^{el\prime}(r^\ddagger)[(1-f^\ddagger) + c_I^{2\ddagger}f^\ddagger]) \quad (5.3)$$

$$K^\ddagger \equiv c_I^{2\ddagger}/c_C^{2\ddagger} = c_I^{2\ddagger}/(1-c_I^{2\ddagger})$$

Equation 5.2 was not explicity derived and discussed in 1, and as we will see provides a new and deeper insight into the conditions

(65) Both terms, $\Delta G_r^{el}/2\hbar\omega_{el}$ and $2k_BT/r^\ddagger$, are smaller than 0.1.

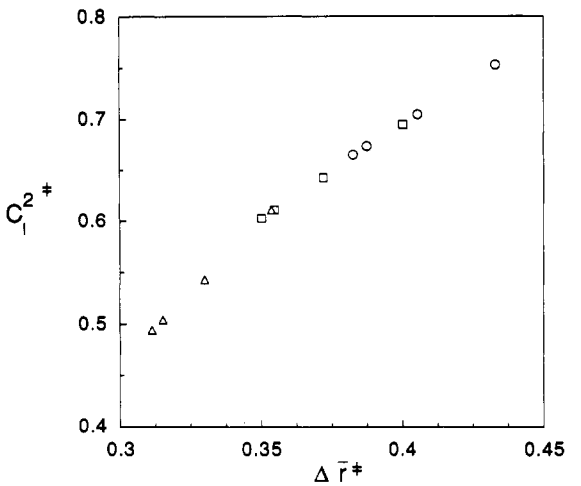

Figure 8. Transition-state character $c_I^{2\ddagger}$ versus relative transition state separation $\Delta\bar{r}^{\ddagger}$ (eq 4.5): (○) *t*-BuCl, (□) *t*-BuBr, (△) *t*-BuI. Although it appears that *t*-BuCl and *t*-BuBr fall on the same line, an approximate relation can be derived[61] which shows the slope for a given substrate is inversely proportional to the TS electronic coupling; thus the slopes for *t*-BuCl and *t*-BuBr are slightly different. After this paper was submitted, Prof. S. Shaik pointed out to us in a private communication that the relative separation parameter $\Delta\bar{r}^{\ddagger}$ has been used previously to assess S_N2 transition-state geometry and activation energy correlations [Shaik, S. S.; Schlegel, H. B.; Wolfe, S. *J. Chem. Soc., Chem. Commun.* **1988**, 1322].

that determine the TS ionic character for S_N1 ionizations. While it may seem imposing, its interpretation is straightforward. The left hand side is composed of the covalent force, $F_C(r^{\ddagger}) = -V_C^{0\prime}(r^{\ddagger})$, the restoring force associated with the covalent *t*-BuX bond stretching, and the coupling variation $\beta'(r^{\ddagger})$. The latter is multiplied by a $c_I^{2\ddagger}$-dependent term which shows that the utilization of the coupling depends on the solute charge distribution, as in eq 2.7. The right hand side of eq 5.2 contains the effective ionic force $F_{I,eff}(r^{\ddagger})$ and a proportionality factor $K^{\ddagger}$, which can be thought of as an effective equilibrium constant determining the TS charge character. $F_{I,eff}(r^{\ddagger})$ is the solvent-mediated effective ionic repulsion and ultimately stems from the tendency of two solvated ions to separate and become stabilized. Note that $F_{I,eff}(r^{\ddagger})$ is smaller in magnitude—due to the multiplicative $c_I^{2\ddagger}$ and $f^{\ddagger}$ factors—than the ionic repulsion between two distinct and fully equilibrated ions, $F_I^{eq}(r) = -\partial G_I^{eq}(r)/\partial r = -(V_I^{0\prime}(r) - \Delta G'_r(r) - \Delta G_r^{el\prime}(r))$. This is to be expected since the actual TS does not correspond to two distinct ions but rather to something closer to 50% ionic (cf. section 4A). In summary, eq 5.2 represents the balancing condition between the reaction system forces; all forces must be equalized in order to obtain the TS. The $K^{\ddagger}$ term on the right hand side of eq 5.2 carries the strongest $c_I^{2\ddagger}$ dependence, so attention will be focused there.

We first use eq 5.2 to characterize the TS ionic character. When the sum of the coupling variation and covalent force is larger than the effective ionic repulsion, $K^{\ddagger}$ must be greater than unity in order to satisfy eq 5.2, and hence $c_I^{2\ddagger} > 1/2$: the TS has a greater than 50% ionic character. Strong covalent forces generally mean the covalent bond is stronger and must be stretched farther before it can break; thus the TS will be more product-like. In the opposite case, namely if $F_{I,eff}(r^{\ddagger})$ is larger than the sum of the coupling variation and covalent force, $K^{\ddagger}$ must be less than unity, so that $c_I^{2\ddagger} < 1/2$. When the effective ionic force so dominates, the TS is less than 50% ionic, corresponding to a more easily broken bond and a more reactant-like TS.[66] Only one case under examination corresponds to this regime, namely *t*-BuI in

(66) The cases $c_I^{2\ddagger} \geq 1$, $c_I^{2\ddagger} \leq 0$ are impossible as the probabilistic aspect of the wavefunction is violated.

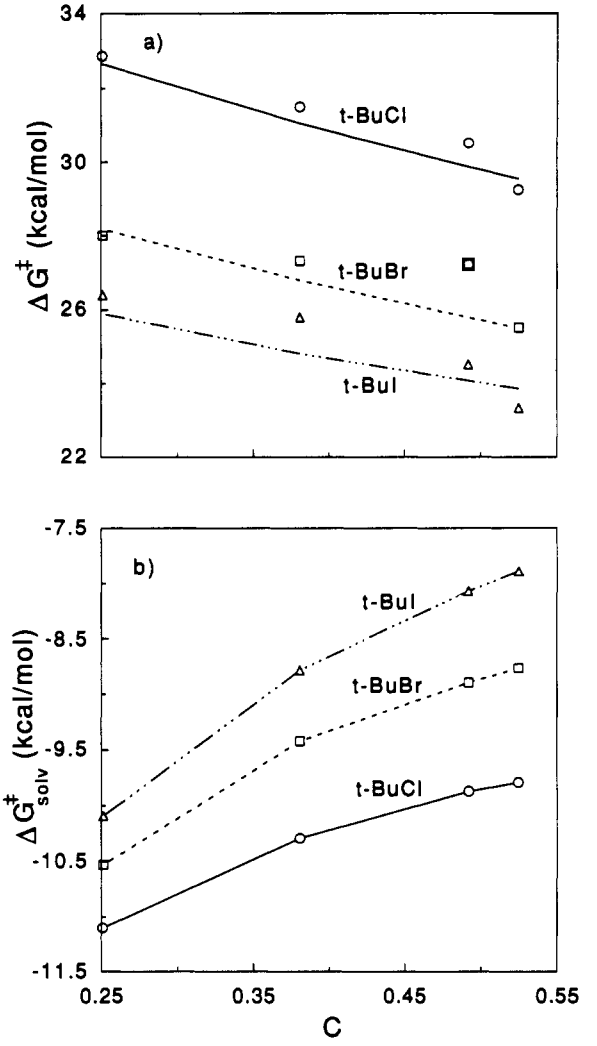

Figure 9. (a) Activation free energies $\Delta G^{\ddagger}$ as a function of solvent polarity factor $C \equiv \epsilon_\infty^{-1} - \epsilon_0^{-1}$. The data points are experimental values taken from ref 3; the lines correspond to the computed values. As discussed in ref 8b, experimental identification of $\Delta G^{\ddagger}$ is somewhat ambiguous; in particular, $\Delta G^{\ddagger}$ is not $-\log k$. The data point for *t*-BuBr in C_6H_5Cl is an estimate. (b) Transition-state solvent stabilization $\Delta G^{eq}_{\ddagger,solv}$ as a function of solvent polarity factor $C \equiv \epsilon_\infty^{-1} - \epsilon_0^{-1}$. The data points correspond to the calculated values for the solvents listed in Figure 7.

CH_3CN (cf. Figures 6c and 7b); in all other cases, the covalent force and coupling variation combination dominates, and the TS ionic character is greater than 50%. Note the effect of the coupling on the TS. The coupling variation $\beta'(r^{\ddagger})$ combines with the covalent force $F_C(r^{\ddagger})$ and pushes towards a larger TS ionic character given the same effective ionic force $F_{I,eff}(r^{\ddagger})$.[8a]

Using eq 5.2, we can now explain the fixed solvent polarity TS trends for the *tert*-butyl halides (cf. Table III). First, one would expect $F_{I,eff}(r^{\ddagger})$ to be largest for *t*-BuCl and smallest for *t*-BuI based on the halide size difference; smaller ions have a greater tendency to separate and become fully solvated than larger ones. At the TSs in CH_3CN, $F_{I,eff}(r^{\ddagger}) \sim 85.3$, ~ 69.2, and ~ 48.4 kcal/mol per Å for *t*-BuCl, -Br, -I, respectively. Second, this decrease of $F_{I,eff}(r^{\ddagger})$ on going from *t*-BuCl to *t*-BuI in a fixed solvent indicates that the ionic character would increase by eq 5.2 *if* the coupling variation and covalent force were constant. But in actuality, the coupling variation is not at all the same for the three halides; it decreases markedly in magnitude $\beta'(r^{\ddagger}) \sim -46.1$, ~ -27.7, and ~ -6.9 kcal/mol per Å. In addition, the covalent force decreases in magnitude because of decreasing BDEs; $F_C(r^{\ddagger}) \sim -48.4$, ~ -41.5, and ~ -36.9 kcal/mol per Å. The combination of these last two features then overwhelms the

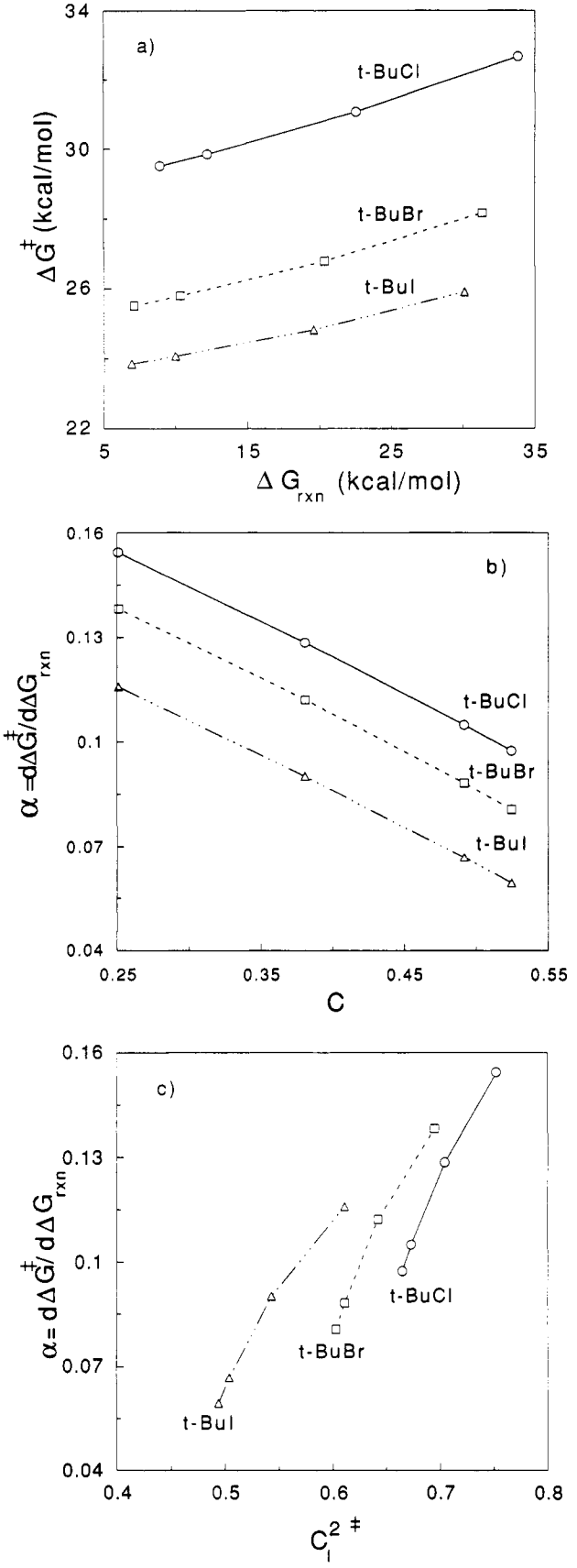

Figure 10. (a) Brønsted plot for activation and reaction free energies, (b) variation of Brønsted coefficient $\alpha = d\Delta G^{\ddagger}/d\Delta G_{rxn}$ with solvent polarity, and (c) correlation of α with transition-state ionic character $c_I^{2\ddagger}$. ΔG_{rxn} is evaluated at 200% ($\Delta\bar{r} = 2$) separation over the respective reactant separations r_{eq}. Data points correspond to calculated values for the solvents in Figure 7. The correlation in (c) is not exactly linear because of the slight variation of the cavity ratio in eq 5.9.

Table IV. Calculated and Experimental Rate Constants[a,b]

	C_6H_5Cl	CH_2Cl_2	$(CH_3)_2CO$	CH_3CN
t-BuCl	10.7	9.5	8.7	8.4
expt	11.3	9.5	9.6	8.6
t-BuBr	7.5	6.5	5.7	5.5
expt		7.2	7.1	5.9
t-BuI	5.9	5.1	4.5	4.4
expt	6.6	6.1	5.2	4.3

[a] $-\log k$, k in s^{-1}. [b] Experimental values taken from ref 3.

decreasing $F_{I,eff}(r^{\ddagger})$ to yield a net decreasing ionic character trend, as observed in Table III. The largest contribution to the change in the series comes from the coupling variation; the decreasing covalent force trend alone is not able to overcome the $F_{I,eff}(r^{\ddagger})$ trend. Now we have a better understanding of the fixed solvent *t*-BuX ionic character trends: since the $\beta(r)$ variation magnitude is highest for *t*-BuCl, it will have the highest TS ionic character. Likewise, *t*-BuBr will be intermediate, and *t*-BuI will have the lowest TS ionic character. The fixed solvent polarity ionic character trend among the halides is thus a result of the decreasing coupling variation (see section 3B for explanation of the coupling trends themselves).

B. Activation Free Energy. Turning now to the activation barrier origin, the activation free energy $\Delta G^{\ddagger}$ is given from eqs 2.7 and 2.14 by

$$\Delta G^{\ddagger} = [V_C^0(r^{\ddagger}) + (V_I^0(r^{\ddagger}) - V_C^0(r^{\ddagger}))c_I^{2\ddagger} - G_R^{eq}] \quad (5.4)$$

$$-2\beta(r^{\ddagger})c_C^{\ddagger}c_I^{\ddagger} + \Delta G_{\ddagger,solv}^{eq} - k_B T \ln [r^{\ddagger}/r_0]^2$$

where the TS solvation free energy $\Delta G_{\ddagger,solv}^{eq}$ is eq 4.2. All quantities here are evaluated at the TS, save the reactant free energy G_R^{eq}. $\Delta G^{\ddagger}$ contains (a) the weighted average of the vacuum covalent and ionic curves minus the reactant free energy, (b) the electronic coupling contribution, and (c) the solvation free energy. (The temperature-dependent rotational term is not important here.) We stress again that in the conventional Hughes–Ingold[2-5] explanation, the decrease of $\Delta G^{\ddagger}$ (cf. Figure 9a) with increasing solvent polarity would have its origin in an increase of the magnitude of $\Delta G_{\ddagger,solv}^{eq}$. However, as already shown in Figure 9b, the magnitude of $\Delta G_{\ddagger,solv}^{eq}$ decreases, so the decrease in $\Delta G^{\ddagger}$ must have its origin in either or both of the remaining contributions to eq 5.4 ((a) and (b) above).

In Figure 11, the three contributions to eq 5.4 are displayed as a function of solvent polarity. As in 1, $\Delta G^{\ddagger}$ decreases for *t*-BuCl as a result *only* of the electronic coupling variation with r; its weighted vacuum contribution does not change appreciably, and the solvent stabilization $\Delta G_{\ddagger,solv}^{eq}$ goes in the wrong direction (cf. Figure 9b). However, for *t*-BuBr and *t*-BuI, Figure 11 shows the increasing importance of the weighted vacuum average in determining the $\Delta G^{\ddagger}$ trend. For *t*-BuBr in Figure 11b, it contributes approximately the same as the electronic coupling. For *t*-BuI in Figure 11c, the electronic coupling contribution is essentially constant, and the variation in the weighted vacuum average is the source of the $\Delta G^{\ddagger}$ decrease. Numerically, this change of origin of the $\Delta G^{\ddagger}$ decrease *is* in part due to the decreasing electronic coupling trend. It is found that the overall solute polarity change in $c_I^{2\ddagger}$ increases as *t*-BuCl < *t*-BuBr < *t*-BuI, in agreement with the TS condition eq 5.2 and Figure 2a: a small electronic coupling variation is less able to cancel the $F_{I,eff}$ variation as solvent polarity is changed. A larger net $c_I^{2\ddagger}$ change results in a larger weighted vacuum change, due to a greater percentage contribution of V_C^0. *t*-BuI should then have the greatest weighted

vacuum change, with *t*-BuBr intermediate, and *t*-BuCl the least. This is what is observed in Figure 11.[67]

In summary, the electronic coupling variation, when large enough, is the source of the $\Delta G^{\ddagger}$ decrease with increasing solvent polarity. *t*-BuCl is the example corresponding to this regime. For *t*-BuI where the electronic coupling variation is small, there is a compensating increase in the weighted vacuum average variation so that $\Delta G^{\ddagger}$ again decreases. *t*-BuBr is intermediate, with both factors contributing. The activation barrier origin scenario displayed in Figure 11 for the *tert*-butyl halides is extremely important: it contrasts explicity with the conventional explanation[2-5] where increasing TS stabilization results in decreasing activation free energies.

C. Brønsted Parameter. Finally, we pass to the explanation of the correlation of the Brønsted parameter α with the TS ionic character, indicated in Figure 10a–c. As extensively discussed in 1, the important role of the electronic coupling and its variation precludes a simple analysis based solely on crossing diabatic curves defined in the limit of zero electronic coupling. We therefore need to employ the electronically adiabatic eq 2.7, according to which the general full polarity derivatives of $\Delta G^{\ddagger}$ and ΔG_{rxn} are given by

$$\frac{d\Delta G^{\ddagger}}{dC} = \frac{\partial G^{\ddagger} dr^{\ddagger}}{\partial r\ dC} + \frac{\partial G^{\ddagger} ds^{\ddagger}}{\partial s\ dC} + \frac{\partial G^{\ddagger}}{\partial C} - \frac{\partial G_R dr_{eq}}{\partial r\ dC} - \frac{\partial G_R ds_{eq}}{\partial s\ dC} - \frac{\partial G_R}{\partial C} \quad (5.5)$$

and

$$\frac{d\Delta G_{rxn}}{dC} = \frac{\partial G_P dr_P}{\partial r\ dC} + \frac{\partial G_P ds_R}{\partial s\ dC} + \frac{\partial G_P}{\partial C} - \frac{\partial G_R dr_{eq}}{\partial r\ dC} - \frac{\partial G_R ds_R}{\partial s\ dC} - \frac{\partial G_R}{\partial C} \quad (5.6)$$

where C is the solvent polarity factor in eq 4.4. (This is a convenient solvent polarity measure because the largest contribution to the $G(r, s)$ variation with solvent polarity comes from the change in the C-dependent reorganization free energy ΔG_r, mainly because the change in ϵ_∞ is small in going from CH_3CN to C_6H_5Cl.) Here G_P, r_P, and s_P are the product free energy, separation, and solvent coordinate values. There are several simplifications that can be made. First, since the TS and reactant locations satisfy eq 4.1, the TS and reactant free energy derivatives with respect to both r and s coordinates vanish. Second, the reactant free energy does not change appreciably with solvent polarity, as indicated in section 4A. If one imposes the additional constraint that the free energy, G_P, is evaluated at large enough r such that dr_P/dC is zero,[68] eqs 5.5 and 5.6 reduce to the simple expressions

$$\frac{d\Delta G^{\ddagger}}{dC} = \frac{\partial G^{\ddagger}}{\partial C} - \frac{\partial G_R}{\partial C} \quad (5.7)$$

$$\frac{d\Delta G_{rxn}}{dC} = \frac{\partial G_P}{\partial C} - \frac{\partial G_R}{\partial C}$$

since ds_P/dC is zero, i.e., the product ion pair always has 100% ionic character. The Brønsted slope α in Figure 10 is then

$$\alpha = \frac{d\Delta G^{\ddagger}}{d\Delta G_{rxn}} = \frac{\partial/\partial C(G^{\ddagger} - G_R)}{\partial/\partial C(G_P - G_R)} \quad (5.8)$$

The $\partial G_R/\partial C$ term will generally vanish in aprotic solvents (*cf.* section 3A). It will however be important in protic solvents such as water, where the decrease in entropy associated with the

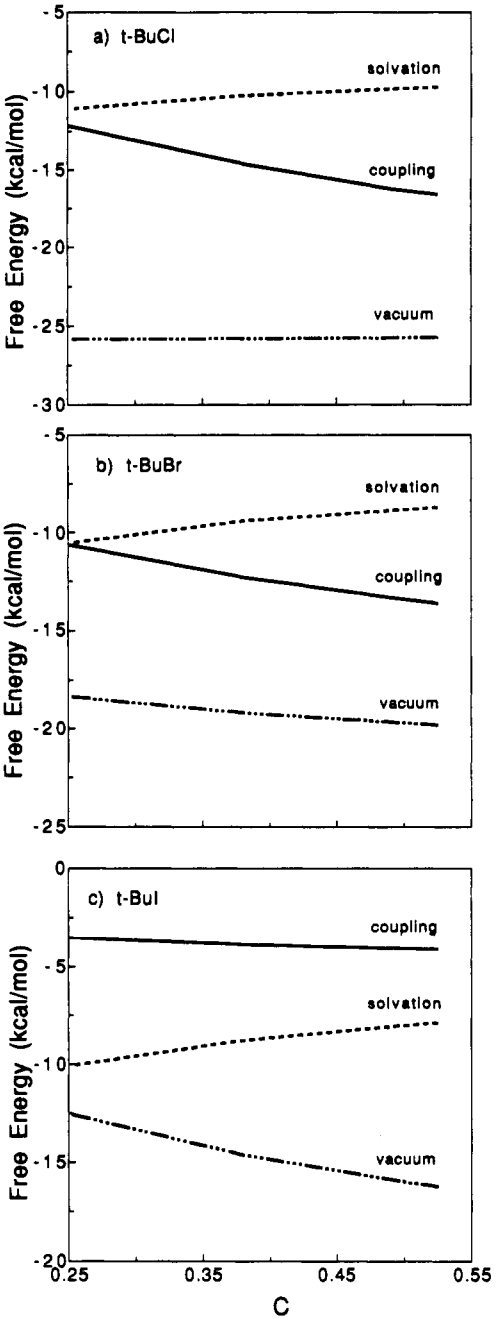

Figure 11. Activation free energy contributions (eq 5.4) for (a) *t*-BuCl, (b) *t*-BuBr, and (c) *t*-BuI as a function of solvent polarity: (– ··· –) vacuum, (—) electronic coupling, and (– –) solvation. The data points correspond to calculated values for the solvents in Figure 7.

(67) Other factors contributing to the increasing importance of the weighted vacuum average to $\Delta G^{\ddagger}$ are the position of $r^{\ddagger}$ for the V_C^0 and V_I^0 curves, the gap $(V_I^0 - V_C^0)$ at that location and how the gap changes as $r^{\ddagger}$ decreases. However, the electronic coupling trend argument in text is the more important factor.

(68) This amounts to making the measurement at some constant r value. It is worthwhile noting again that this procedure is not applicable to an analysis for Figure 5a. There, product free energies are compared for different leaving groups in a fixed solvent, and G_P does not change continuously for the series.

(69) The general expression is

$$\frac{\partial G}{\partial C} = -M_s(r)s^2 - \frac{1}{2}\Delta V(r, s)\frac{\partial x}{\partial C} - \beta(r)\frac{\partial y}{\partial C} + \frac{1}{4}\Delta G_r^{el}(r)y\rho\frac{\partial y}{\partial C}\left(\frac{y + 2\rho}{(y + \rho)^2}\right)$$

Using the Born–Oppenheimer Schrödinger equation in ref 20 to solve for $\partial x/\partial C$ and $\partial y/\partial C$ results in an exact cancellation of the second and third terms on the right hand side. The remaining ρ-dependent solvation term is small numerically for the present cases and can be safely neglected at both the TS and product states.

(70) Using $\Delta\mathcal{F} = 2$ gave the best agreement (better than 5%).

(71) For example, when $\Delta\mathcal{F} = 2$, there is a ~16%, 17%, and 11% variation $M_s^{\ddagger}/M_s^{P}$ for *t*-BuCl, -Br, and -I, respectively. The corresponding variation in $c_I^{4\ddagger}$ is ~23%, 25%, and 37%. α components for all product definitions mentioned in ref 55 were also investigated and gave similar results. Use of $\Delta\mathcal{F} \geq 1$ to evaluate ΔG_{rxn} here serves as a more convenient choice for illustration.

ordering of the water molecules[15] will increase the reactant free energy. Such a patently microscopic phenomenon cannot be adequately described using a dielectric continuum,[13,14] so we restrict attention—as indicated in the Introduction—to aprotic solvents where $\partial G_R/\partial C$ vanishes.

Using eq 2.7 to evaluate eq 5.8 and neglecting terms proportional to f[9,69] gives the simple relation

$$\alpha = \frac{dG^{\ddagger}}{d\Delta G_{rxn}} = \frac{\Delta G^{eq}_{\ddagger,solv}}{\Delta G^{eq}_{P,solv}} \approx \left(\frac{M_s^{\ddagger}}{M_s^{P}}\right) c_I^{4\ddagger} \qquad (5.9)$$

where M_s is given by eq 2.9. The quantity $M_s^{\ddagger}/M_s^{P}$ represents that contribution to the ratio of the free energies of solvation associated with the cavity sizes at the TS and products, respectively. Thus, the slope of a Brøsted plot is approximately equal to the ratio of the solvation free energies at the TS and product states and is also proportional to the square of the TS ionic character. This equation shows explicitly why α is not[8a] the same as the ionic character but is smaller first due to the dependence on the square of $c_I^{2\ddagger}$ and second due to the fact that $M_s^{\ddagger}/M_s^{P} < 1$ because the solute cavity size at the TS is smaller than that of two distinct ions.

The applicability of eq 5.9 for the Brønsted slope has been checked numerically, using $\Delta\bar{r} = 1, 2, 3$ (cf. eq 4.3), and the agreement between the actual $c_I^{2\ddagger}$'s and the calculated values is better than 8% for all halides in all solvents for all values of $\Delta\bar{r}$.[70] Further, the variation of the cavity ratio $M_s^{\ddagger}/M_s^{P}$ (which is due mostly to M_s^{P}) in the solvents listed in section 3A is approximately 1.4–3 times smaller than the variation of the ionic character term $c_I^{4\ddagger}$ for a given value of $\Delta\bar{r}$.[71] Therefore *α directly reflects the TS ionic character*. We then predict that the slope of an experimental Brønsted plot log k vs log K_{eq}, where k is the rate constant and K_{eq} is the equilibrium constant for the reactant–ion-pair product equilibrium, will decrease with increasing solvent polarity,[8a] due to the decreasing ionic character of the TS. This provides a potential experimental test of the novel TS ionic character trend prediction.

6. Concluding Remarks

We have employed a quantum two valence bond state Hamiltonian combined with a dielectric continuum solvent description to analyze S_N1 ionic dissociations for the series *tert*-butyl chloride, -bromide and -iodide is solvents of varying polarity (cf. section 2). The resulting two-dimensional free energy surfaces in Figure 3, in terms of a collective solvent coordinate s and internuclear separation r, allows for a detailed transition state (TS) structure and activation free energetics examination.

The results and their interpretations given here agree with and significantly extend the initial work presented in ref 8a, where only *tert*-butyl chloride ionization was analyzed. Of special importance is the prediction of decreasing TS solvent stabilization with increasing solvent polarity for the *tert*-butyl halide series, i.e., the TS ionic character and separation *decrease* (cf. Figure 7), and that the calculated activation free energy $\Delta G^{\ddagger}$ decreases with increasing solvent polarity *despite* the decreasing TS stabilization (cf. Figure 9). The decrease in $\Delta G^{\ddagger}$ was shown to arise from the variations in the electronic coupling between the covalent and ionic states[8a] and in the vacuum covalent and ionic potentials, with the magnitude of the electronic coupling determining which contribution is more important[67] (cf. Figure 11). This new view of S_N1 ionizations is in total contrast to the conventional Hughes–Ingold[2-5] explanation, where an ionic TS is supposed to be more stabilized in a higher polarity solvent, which is then supposed to account for the experimentally observed decreasing $\Delta G^{\ddagger}$ trend.

We have argued for a possible experimental probe of these theoretical predictions: the slope α of a Brønsted plot,[51] log k vs K_{eq}, where k is the first-order ionization rate constant and K_{eq} is the reactant–ion-pair equilibrium constant, for a given *tert*-butyl halide should decrease with increasing solvent polarity (cf. Figure 10). That the decrease of α is due to decreasing TS ionic character has been established analytically in eq 5.9.

It has also been shown using a force-balance relation (eq 5.2) that the calculated decreasing electronic coupling variation (Cl > Br > I, cf. Figure 2a) is responsible for the TS structure and activation trends for the *tert*-butyl halide series in a fixed solvent, with *tert*-butyl chloride having the greatest ionic character, relative internuclear separation and activation free energy, *tert*-butyl bromide intermediate, and *tert*-butyl iodide the least (cf. Table III). The role played by the electronic coupling in determining these trends provides a perspective fundamentally different from the traditional view.[1,50] In addition, a Brønsted plot[51] for the halide series in a fixed solvent (cf. Figure 5) is shown to have a slope consistent with the Hammond postulate.[47-49] The slope is greater than unity, although sources believed to be responsible for such behavior are not present here.[54] We have also established that an approximately linear correlation exists between TS ionic character and relative TS internuclear separation $\Delta\bar{r} = (r^{\ddagger} - r_{eq})/r_{eq}$ (cf. eq 4.3 and Figure 8), where r_{eq} is the equilibrium reactant bond length, which is at variance with suggestions in the literature for other systems.[62]

Acknowledgment. This work was supported in part by NSF Grant CHE88-07852.